

UC Irvine

UC Irvine Previously Published Works

Title

The spatial chronnectome reveals a dynamic interplay between functional segregation and integration.

Permalink

<https://escholarship.org/uc/item/9q9919r5>

Journal

Human brain mapping, 40(10)

ISSN

1065-9471

Authors

Iraji, Armin
Deramus, Thomas P
Lewis, Noah
et al.

Publication Date

2019-07-01



DOI

10.1002/hbm.24580

Peer reviewed

RESEARCH ARTICLE

The spatial chronnectome reveals a dynamic interplay between functional segregation and integration

Armin Iraj¹  | Thomas P. Deramus¹ | Noah Lewis¹ | Maziar Yaesoubi¹  | Julia M. Stephen¹ | Erik Erhardt² | Aysneil Belger³ | Judith M. Ford^{4,5} | Sarah McEwen⁶ | Daniel H. Mathalon^{4,5} | Bryon A. Mueller⁷ | Godfrey D. Pearlson⁸ | Steven G. Potkin⁹ | Adrian Preda⁹ | Jessica A. Turner¹⁰ | Jatin G. Vaidya¹¹ | Theo G. M. van Erp¹² | Vince D. Calhoun^{1,8,13}

¹The Mind Research Network, Albuquerque, New Mexico

²Department of Mathematics and Statistics, University of New Mexico, Albuquerque, New Mexico

³Department of Psychiatry, University of North Carolina, Chapel Hill, North Carolina

⁴Department of Psychiatry, University of California San Francisco, San Francisco, California

⁵Psychiatry Service, San Francisco VA Medical Center, San Francisco, California

⁶Department of Psychiatry and Biobehavioral Sciences, University of California Los Angeles, Los Angeles, California

⁷Department of Psychiatry, University of Minnesota, Minneapolis, Minnesota

⁸Department of Psychiatry, Yale University, School of Medicine, New Haven, Connecticut

⁹Department of Psychiatry and Human Behavior, University of California Irvine, Irvine, California

¹⁰Department of Psychology, Georgia State University, Atlanta, Georgia

¹¹Department of Psychiatry, University of Iowa, Iowa City, Iowa

¹²Clinical Translational Neuroscience Laboratory, Department of Psychiatry and Human Behavior, University of California Irvine, Irvine, California

¹³Department of Electrical and Computer Engineering, University of New Mexico, Albuquerque, New Mexico

Correspondence

Armin Iraj¹ and Vince D. Calhoun, The Mind Research Network, 1101 Yale Blvd NE, Albuquerque, NM 87106, USA.

Emails: armin.iraji@gmail.com; vcalhoun@mrn.org

Funding information

National Institute of Mental Health, Grant/Award Number: R01MH058262; National Institutes of Health, Grant/Award Numbers: 2R01EB005846, P20GM103472, R01REB020407; National Science Foundation, Grant/Award Number: 1539067; U.S. Department of Veterans Affairs, Grant/Award Number: I01 CX0004971

Abstract

The brain is highly dynamic, reorganizing its activity at different interacting spatial and temporal scales, including variation within and between brain networks. The chronnectome is a model of the brain in which nodal activity and connectivity patterns change in fundamental and recurring ways over time. Most literature assumes fixed spatial nodes/networks, ignoring the possibility that spatial nodes/networks may vary in time. Here, we introduce an approach to calculate a spatially fluid chronnectome (called the spatial chronnectome for clarity), which focuses on the variations of networks coupling at the voxel level, and identify a novel set of spatially dynamic features. Results reveal transient spatially fluid interactions between intra- and internetwork relationships in which brain networks transiently merge and separate, emphasizing dynamic segregation and integration. Brain networks also exhibit distinct spatial patterns with unique temporal characteristics, potentially explaining a broad spectrum of inconsistencies in previous studies that assumed static networks. Moreover, we show anticorrelative connections to brain networks are transient as opposed to constant across the entire scan. Preliminary assessments using a multi-site dataset reveal the ability of the approach to obtain new information and nuanced alterations that remain undetected during static analysis. Patients with schizophrenia (SZ) display transient decreases in voxel-wise network coupling within visual and auditory networks, and higher intradomain coupling variability. In summary, the spatial chronnectome represents a new direction of research enabling the study of functional networks which are transient

at the voxel level, and the identification of mechanisms for within- and between-subject spatial variability.

KEYWORDS

brain spatial dynamics, dynamic segregation and integration, large-scale networks, resting state fMRI (rsfMRI), schizophrenia, spatial chonnectome, spatial coupling, spatial states, spatiotemporal transition matrix

1 | INTRODUCTION

Neuroimaging modalities provide unique opportunities to model and investigate brain functional connectivity at a large/macro scale. One key finding is a set of replicable large-scale functional brain networks (Biswal et al., 2010; Buckner et al., 2009; Franco, Pritchard, Calhoun, & Mayer, 2009; Guo et al., 2012; Shehzad et al., 2009; Zuo et al., 2010). Brain networks and groups of temporally coherent activity within networks, called functional domains, have been studied and validated using various analytical approaches (Calhoun, Kiehl, & Pearson, 2008; Smith et al., 2009; van den Heuvel, Mandl, Kahn, & Hulshoff Pol, 2009; Van Dijk et al., 2010; Yeo et al., 2011). Of these approaches, independent component analysis (ICA) enables simultaneous extraction of both the spatial patterns of functional domains and their temporal activity. Studies of brain networks and functional domains demonstrate alterations in their spatial/temporal patterns under different physiological and psychological conditions (Arbabshirani, Plis, Sui, & Calhoun, 2017; Garrity et al., 2007; Greicius, 2008; Iraj et al., 2015; Menon, 2011; Seeley, Crawford, Zhou, Miller, & Greicius, 2009; Sorg et al., 2007). However, these studies hold a common assumption that each brain network is comprised of a fixed set of brain regions with a static pattern of activity over time. This is an oversimplification, as the brain is highly dynamic, with variations in associated regions and spatial patterns of brain functional organizations including brain networks (Calhoun, Miller, Pearson, & Adali, 2014). As such, many recent studies have demonstrated the ability of fMRI to capture time-varying brain connectivity (Calhoun et al., 2014; Hutchison et al., 2013; Preti, Bolton, & Van De Ville, 2017). For instance, studying whole-brain dynamic connectivity demonstrates variations in temporal coupling, both within and between functional domains (Allen et al., 2014; Damaraju et al., 2014). Examining temporal coupling between brain regions reveals strong correlations between regions known to be part of one network with regions of other networks at particular moments in time. This suggests “isolated” brain networks are only transiently isolated. Additionally, despite recent developments in detecting the dynamic behavior of brain activity using fMRI, spatio-temporal variations of brain networks have been underappreciated. Previous time-varying studies have focused on either (a) dynamic temporal coupling among fixed spatial nodes/networks, which ignore the importance of spatial variations (Allen et al., 2014; Barttfeld et al., 2015; Chen, Cai, Ryali, Supekar, & Menon, 2016; Ciric, Nomi, Uddin, & Satpute, 2017; Damaraju et al., 2014; Hutchison et al., 2013; Leonardi et al., 2013; Sakoglu et al., 2010; Shine, Koyejo, & Poldrack, 2016;

Yaesoubi, Adali, & Calhoun, 2018) or (b) the dominant spatial pattern at any given timepoint. While these approaches highlight snapshots of spatial patterns at the voxel level, they do not capture the dynamics of spatial variation within and between co-evolving functional networks (Karahanoğlu & Van De Ville, 2015; Liu & Duyn, 2013; Preti & Van De Ville, 2017; Tagliazucchi, Balenzuela, Fraiman, & Chialvo, 2012; Trapp, Vakamudi, & Posse, 2018; Vidaurre, Smith, & Woolrich, 2017). Kiviniemi and his colleagues presented work highlighting spatial variation in the default mode network using sliding-window ICA (Kiviniemi et al., 2011). Other work investigated fluctuation in spatial couplings between spatial components derived from independent vector analysis (Ma, Calhoun, Phlypo, & Adali, 2014). While these present intriguing early evidence, to date with the exception of our recent work (Iraj et al., 2018), there has not been an approach that evaluating the spatial fluidity within and/or between functional brain networks. Spatial fluidity is defined as the transitory spatial pattern of a given functional organization over time at the finest scale or measurement (voxels). Spatially fluid brain networks evolve in their voxel-wise spatial patterns over time which includes their integration and separation with one another.

The chonnectome is a model of the brain in which nodal activity and connectivity patterns change in fundamental and recurring ways through time (Calhoun et al., 2014). Here, we introduce an approach allowing for a spatially fluid chonnectome (called the *spatial chonnectome*) which advances current analytical methods by providing novel, space/time-varying information of individual brain networks at the voxel level. Encapsulating transient voxel-wise network coupling allows researchers to capture the spatially fluid behaviors of brain networks. To investigate the spatiotemporal variations of brain networks, we calculate the relationship (via temporal correlation) of each individual brain network with every voxel of the brain. Because the time course of each brain network obtained from ICA represents the network's temporal activity, its temporal correlation with each brain voxel provides information about the involvement of the voxel with the brain network. Using correlation (rather than multiple regression) allows us to capture the association of each voxel to a given network to a full extent regardless of its contribution to other networks. The spatiotemporal variations of a brain network were encapsulated through measuring the coupling (temporal correlation) between every brain voxel and the given brain network at different moments using a sliding-window approach. Preliminary assessments demonstrate that spatial patterns of brain networks evolve continuously over time and also highlight the ability of the approach to obtain new information of brain function. A new set of spatially relevant features can be

calculated and used to study brain function. For instance, we introduce a metric called the “spatiotemporal transition matrix” to summarize the spatiotemporal information of each brain network. For each brain network, we also characterize distinct, highly replicable spatial states with unique temporal characteristics. Using spatial states, the dynamic properties of each brain network can also be assessed by calculating temporally derived indices such as mean dwell time or fraction time for individual brain networks (Damaraju et al., 2014).

It is worth mentioning that the spatial states are also related to NC states (temporally network connectivity states) identified by utilizing the time courses of intrinsic connectivity networks (ICNs) associated with a given large-scale network (Ciric et al., 2017). However, the spatial states take advantage of both spatial and temporal information to estimate distinct spatial dynamic patterns of a given brain network. The spatial states of large-scale networks can also be related to interdigitated networks previously only observed in single subject analysis (Braga & Buckner, 2017; Laumann et al., 2015). The goal of this study is to introduce the spatial chronnectome and propose several novel spatial dynamic features. We also demonstrate the utility of the spatial chronnectome by evaluating the sensitivity of spatial chronnectome properties to differences between schizophrenia (SZ) patients versus healthy controls. We hypothesized that the spatial chronnectome would allow us to detect nuanced and meaningful alterations in the brain networks of patients with SZ which would not be detected during static analyses. Results show that transient decreases in voxel-wise networks couplings are significantly more pronounced than reductions in static functional connectivity. Furthermore, our approach detected alterations in brain networks that are not identified when a spatially static analysis was performed. Using a variation-based analysis, we demonstrate, for the first time, high coupling variability and different spatiotemporal transition patterns across various brain networks. We conclude that utilizing the spatial aspects of brain dynamics, which have been overlooked by focusing on variations in temporal coupling among fixed spatial nodes/networks, can unveil typically overlooked features of the dynamic brain and potentially improve our understanding of cognitive and behavioral neuroscience.

2 | METHODS

2.1 | Outline of our approach

Our approach assessing spatiotemporal variations of individual brain networks includes the following steps (Figure 1a):

1. Spatial independent component analysis (sICA) is applied to obtain large-scale brain networks and their associated time courses (Figure 1a Step 1). The time course of each brain network obtained from sICA represents the temporal activity of that large-scale brain network. Details can be found in Section 2.4. Identifying large-scale brain networks: Spatial ICA.
2. Temporal coupling and sliding-window approaches were employed to capture spatiotemporal variations of the large-scale brain networks. For each brain network and time window, we calculated the correlation between the time course of the brain network and the time

courses of every voxel of the brain. The resulting correlation values represent the association (involvement) of all voxels across the brain to the given network at each time window (Figure 1a Step 2). This results in one dynamic coupling map (dCM) per window for each brain network. This approach, unlike its predecessors, such as whole brain dynamic functional network connectivity (dFNC) and co-activation patterns (CAP), provides nuanced information regarding temporal variations of spatial patterns of multiple brain networks simultaneously at the level of the voxel. Details can be found in Section 2.5. Calculating dCMs for each brain network using a sliding-window approach.

3. Time-varying properties were evaluated for each brain network (Figure 1a Step 3). First, the dCMs of each individual network were clustered into a set of distinct spatial patterns called spatial states on which multiple dynamic metrics were calculated and investigated (see Section 2.6. Calculating the spatial states of each brain network and their dynamic patterns). Next, the spatially-continuous variations of each brain network over time were evaluated by calculating voxel-wise changes in their dCMs (See Section 2.7. Evaluating the spatial variations of each brain network over time).

2.2 | Data collection

Data collection was performed at 7 imaging sites across the United States, and all analyzed data passed data quality control. All participants are at least 18 years old and gave written informed consent prior to enrollment. Data were collected from 160 healthy participants, including 46 females and 114 males (average age: 36.71 ± 10.92 ; range: 19–60 years), and 149 age- and gender-matched patients with SZ, including 36 females and 113 males (average age: 37.95 ± 11.47 ; range: 18–60 years). The imaging data were collected on a 3-Tesla Siemens Tim Trio scanner for six of the seven sites and on a 3-Tesla General Electric Discovery MR750 scanner at one site. Resting state fMRI (rsfMRI) data were acquired using a standard gradient echo-planar imaging (EPI) sequence with following imaging parameters: repetition time (TR) = 2,000 ms, echo time (TE) = 30 ms, flip angle (FA) = 77° , field of view (FOV) = 220×220 mm, matrix size = 64×64 , mm, pixel spacing size = 3.4375×3.4375 mm, slice thickness = 4 mm, slice gap = 1 mm, number of excitations (NEX) = 1, and a total of 162 volumes. During rsfMRI scans, participants were instructed to keep their eyes closed and rest quietly without falling asleep. Further details on this dataset can be found in our earlier work (Damaraju et al., 2014).

2.3 | Preprocessing

The preprocessing was performed primarily using SPM (<http://www.fil.ion.ucl.ac.uk/spm/>) and AFNI (<https://afni.nimh.nih.gov>) software packages. The pipeline includes brain extraction, motion correction using the INRIAlign, slice-timing correction using the middle slice as the reference time frame, and despiking using AFNI's 3dDespike. The data of each subject was subsequently warped to the Montreal Neurological Institute (MNI) template using nonlinear registration, resampled to 3 mm^3 isotropic voxels, and spatially smoothed using a Gaussian kernel with a 6 mm full width at half maximum (FWHM = 6 mm). Finally, voxel time courses were

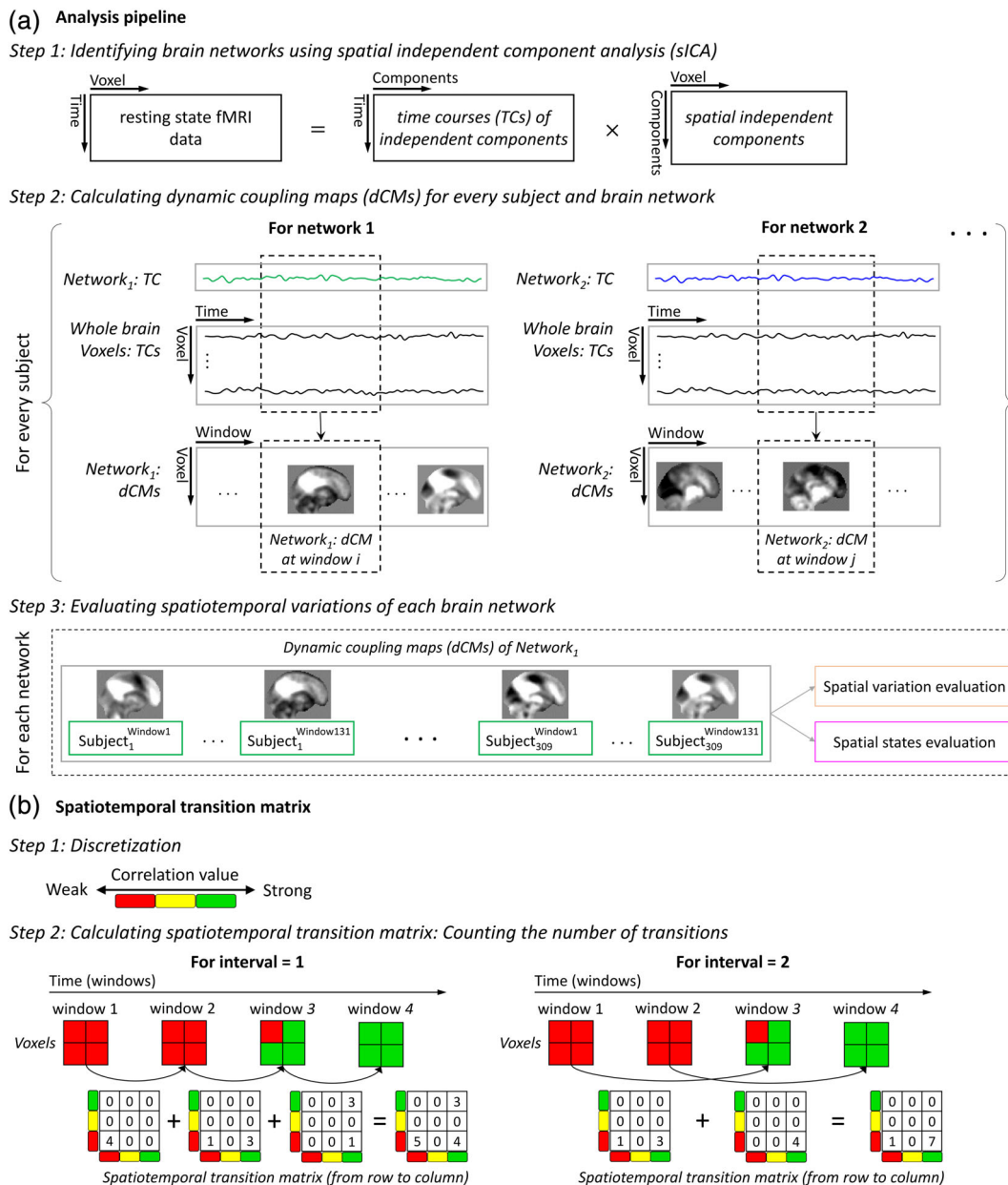


FIGURE 1 Summary of processing steps. (a) Cartoon of the analysis pipeline. First, spatial independent component analysis (sICA) is applied to obtain brain networks and their associated times courses. ICA consists of several steps including data reduction (PCA), group-level sICA, and subject-level sICA. Following ICA, whole brain dCMs of each network for every subject are obtained by calculating windowed-correlation values between the time course of the network and every brain voxel. Finally, time-varying properties of each network are investigated by evaluating spatial variation of dCMs over time and estimating spatial states. Details of the spatiotemporal variation analysis can be found in Sections 2.6 and 2.7. (b) a toy model of calculating the spatiotemporal transition matrix. First, we discretize the correlation value. For visualization purpose, we present three bins here. However, 10 bins were used in the analysis of the real data in which each bin represents a range of correlation value (e.g., 0.2–0.3). Next, we count the number of transitions from one bin to another between time windows at a given interval. An interval of one refers to evaluating changes between consecutive spatiotemporal transition matrices. An interval of two evaluated changes between every two spatiotemporal transition matrices with distance equal to two TRs

z-scored (variance normalized) as it has been shown in our analysis to better estimate brain networks relative to other scaling methods for ICA.

2.4 | Identifying large-scale brain networks: Spatial ICA

Spatial ICA (sICA) was applied to the fMRI data to obtain brain networks (Calhoun & Adali, 2012; Calhoun, Adali, Pearlson, & Pekar,

2001a). ICA was performed using the GIFT software package (<http://mialab.mrn.org/software/gift/>) in the following steps similar to our previous work (Iraji et al., 2016): (a) Subject-level principal component analysis (PCA) was applied and the 30 principal components accounting for the maximum variance in each individual dataset were retained. (b) All subject-level principal components were concatenated together across the time dimension, and group-level spatial PCA was applied on 9,270 (30 × Subject) concatenated components. (c) The

first 20 group-level principal components with the highest variance were selected as input for the infomax algorithm to estimate the 20 group independent components (Bell & Sejnowski, 1995; Correa, Adali, & Calhoun, 2007; Correa, Adali, Li, & Calhoun, 2005). Infomax ICA algorithm was repeated 100 times on the 20 group-level principal components using ICASSO framework in order to obtain a stable and reliable estimation of independent components (Himberg, Hyvarinen, & Esposito, 2004), and the most representative run was selected for further analysis (Ma et al., 2011). (d) The subject-specific independent components and component time courses were calculated using group information guided ICA (GIG-ICA; Du et al., 2015; Du & Fan, 2013). (e) The 12 independent components were identified as brain networks based on the spatial and temporal properties and prior knowledge from previous studies.

2.5 | Calculating dCMs for each brain network using a sliding-window approach

The spatiotemporal variations of each brain network can be captured by evaluating its dynamic coupling at a voxel-wise level. For this purpose, we calculated the temporal coupling between the brain network and every voxel of the brain using the sliding-window correlation approach. Temporal correlations have been used as the primary metric to measure functional connectivity, fully capturing the relationship between a given voxel and the brain network without regard to its contributions of other networks. For instance, if a given voxel is highly correlated with two networks, using correlation allows detecting both of these associations. As a result, we compute dCMs for a given network, which encapsulates the spatiotemporal variations of that brain network at a voxel-wise level. The same cleaning procedure that has previously demonstrated its effectiveness in improving the detection of dynamic patterns (Allen et al., 2014; Damaraju et al., 2014) was first performed on the time courses of brain networks and every voxel of the brain to reduce noise. The cleaning procedure includes orthogonalizing with respect to estimated subject motion parameters, linear detrending, despiking, and band-pass filtering using a fifth-order Butterworth filter (0.01–0.15 Hz). It is worth mentioning that to evaluate the noise effect, we performed various cleaning procedures including various bandpass filtering methods with different frequency bands, and these approaches resulted in almost identical spatial states. Further details of different cleaning procedures can be found in our recent work (Iraji et al., 2018). We used the tapered window obtained by convolving a rectangle (width = 30 TRs; see the discussion for our reasoning for the specific window length chosen) with a Gaussian ($\sigma = 3$ TRs) and the sliding step size of one TR resulting in 131 windows per subject (Allen et al., 2014; Damaraju et al., 2014). The spatial evolution (i.e., continuous spatial variations) of brain networks were evaluated using different metrics including spatial states and spatiotemporal variation analyses.

2.6 | Calculating the spatial states of each brain network and their dynamic patterns

First, we modeled the spatiotemporal fluctuations of each brain network as temporal variations in a set of distinct spatial patterns called

spatial states. Clustering approaches can be used to summarize the dCMs of each brain network into a set of spatial states which allows us to investigate the spatiotemporal variations of the brain network via temporal variations of these distinct spatial states. Here, *k*-means clustering was employed to detect the spatial states of each brain network. For each brain network, *k*-means clustering was applied on the 40,479 (309 subjects \times 131 windows) dCMs of the brain network. *k*-means clustering was repeated 100 times with different initializations using the *k*-means++ technique to increase chances of escaping local minima (Arthur & Vassilvitskii, 2007). The correlation distance metric was used to measure the similarity between data points (i.e., the dCMs), as it is more effective in the detection of spatial patterns irrespective of voxel intensities. However, an exploratory analysis using Euclidean distance demonstrated almost identical results. *k*-means clustering was performed for 3–10 clusters, and the spatial maps of the cluster centroids were compared (Supporting Information S1). For each brain network, the maximum number of clusters that provides distinct spatial maps for centroids were selected by visual inspection for further analysis. Thus, each network includes multiple spatial states as defined by the cluster centroids, and the number of spatial states (centroids) can vary between networks. We also compared our numbers of clusters with the estimated number of clusters using the elbow criterion (Damaraju et al., 2014; Yaesoubi, Miller, & Calhoun, 2017). With the exception of the left frontoparietal and subcortical domains, in which the elbow criterion estimates a higher number of clusters than those chosen by visual inspection, the estimated cluster numbers using elbow criterion were the same as the expert selections. Using temporal profiles of the spatial states, various state level and meta-state level dynamic indices can be calculated for each brain network. For example, the mean dwell time (the average of the amount of time that subjects stay in a given state once entering that state) and the fraction time (the proportion of time subjects stay in a given state) can be calculated for each networks. Here, we compared mean dwell time and fraction time between healthy subjects and patients with SZ to show the feasibility of the approach.

2.7 | Evaluating the spatial variations of each brain network over time

2.7.1 | Coupling variability map

Coupling variability for each network is defined as the amount of variations in network coupling over time, which is obtained by measuring voxel-wise changes in dCMs using the L1 norm distance (sum of absolute differences). For each voxel, the L1 norm distance represents the variations in a voxel's membership to a given brain network over time by measuring changes in the sliding-window correlation values between the time courses of a given voxel and the brain network across time. For example, if the correlation values for a given voxel for seven consecutive time windows are $c_1, c_2, \dots,$ and c_7 , the changes in correlation values will be $d_1 = |c_2 - c_1|, d_2 = |c_3 - c_2|, \dots, d_6 = |c_7 - c_6|$. Therefore, the coupling variability for a given voxel will be equal to $d_1 + d_2 + \dots + d_6$ (Supporting Information S2). The coupling variability map quantifies the overall spatial behavior of a given brain network varying across time. Voxel-wise comparisons were further applied

comparing coupling variability maps for each network between healthy subjects and patients with SZ.

2.7.2 | Spatiotemporal transition matrix

To further evaluate spatiotemporal variations of each brain network, we exploit the gray-level co-occurrence (spatial dependence) matrix method in the field of image processing that is used to extract Haralick textural features from images (Haralick, Shanmugam, & Dinstein, 1973). Figure 1b shows a toy model of this approach. First, the network coupling (i.e., voxel-to-network correlation) values are discretized to n bins (10 equal bins in this study). The spatiotemporal transition matrix is constructed by counting the number of voxels transitioning from one bin to another between time windows at a given interval. We calculate this spatiotemporal transition matrix for an interval of one TR, (i.e., by counting the number of transitions between every two consecutive spatial maps), and for larger intervals. The maximum interval would be the total number of windows per subject minus 1 (i.e., 130). The spatiotemporal transition matrix was normalized (divided) by the total number of transitions to allow us to compare across different interval values. Several global indices such as contrast, correlation, energy, entropy, and homogeneity can be calculated from spatiotemporal transition matrix to provide summary statistics of spatiotemporal variations of brain networks (Haralick et al., 1973). Here, for example, the energy index was calculated to evaluate spatiotemporal uniformity. The energy index, also known as angular second moment (ASM), is defined as $\sum_{i,j} p(i,j)^2$ where $p(i,j)$ is the $(i,j)^{\text{th}}$ element of the spatiotemporal transition matrix. The energy index is between zero and one, and smaller energy values represent higher spatiotemporal uniformity. The energy index of each network was compared between healthy subjects and patients with SZ. The energy indices of the networks which show significant differences between the two groups were further analyzed to understand the relationships between the spatiotemporal variations and cognitive scores. For this purpose, we used the domains of the computerized multiphasic interactive neurocognitive system (CMINDS) scores including speed of processing, attention/vigilance, working memory, verbal learning, visual learning, and reasoning/problem solving. Further details of CMINDS and preprocessing steps can be found in (van Erp et al., 2015).

2.8 | Statistical analysis: Dynamic alterations among patients with SZ

The spatiotemporal variations of brain networks were evaluated by comparing group differences between patients with SZ and healthy subjects, and statistical comparisons for each analysis were separately corrected for multiple comparisons based on the total number of comparisons that we performed in that analysis. P -values of all statistical analyses were corrected for multiple comparisons using the 5% false discovery rate (FDR) (Benjamini & Hochberg, 1995). For each statistical comparison, we used a general linear model (GLM) that included age, gender, site, and the mean framewise displacement (meanFD) as covariates. MeanFD was added as a covariate to mitigate against the effects of motion (Power, Barnes, Snyder, Schlaggar, & Petersen, 2012). To evaluate the relationship between energy indices and CMINDS scores, correlation analyses were conducted separately for

healthy subjects and patients with SZ after regressing out age, gender, site, and meanFD. CMINDS scores and energy indices were mean-centered for each group to mitigate group differences in either CMINDS scores and/or energy indices introduced into the correlations. The group difference in correlation coefficients of the relationship between energy indices and CMINDS scores was also evaluated between the two groups. Outliers were removed using the scaled median absolute deviation.

3 | RESULTS

3.1 | Large-scale brain networks

We applied spatial ICA with 20 components on rsfMRI data from 309 individuals. The ICA algorithm ran several times and clustering the resulting components revealed a high level of compactness (a cluster quality index greater than 0.8), indicating the reliability of the independent components (Himberg et al., 2004). Twelve independent components were identified as neuronal activity related components, or brain networks (Erhardt, Allen, Damaraju, & Calhoun, 2011), based on their temporal and spatial properties and knowledge from previous studies. The time courses of the selected components are dominated by low-frequency fluctuations, which were evaluated using the dynamic range and the ratio of low-frequency to high-frequency power (Allen et al., 2011). Their spatial maps have significant overlap with gray matter, their peak activations fall within gray matter, and low spatial overlap with known ventricular, motion, and susceptibility artifact components (Allen et al., 2011). Furthermore, the selected components have high spatial similarity with one of the established ICNs (Allen et al., 2011; Beckmann, DeLuca, Devlin, & Smith, 2005; Damoiseaux et al., 2006; Fox, Corbetta, Snyder, Vincent, & Raichle, 2006; Irajii et al., 2016; Smith et al., 2009; Yeo et al., 2011; Zuo et al., 2010). The identified brain networks are the auditory, cerebellar, default mode, (dorsal) attention, left and right frontoparietal, somatomotor, language, salience, subcortical, primary visual, and secondary visual networks (Figure 2). The group spatial maps of networks obtained from the full dataset were used as the reference to calculate the spatial maps of networks and their associated time courses for each individual. This procedure prevents biasing the spatial maps of networks toward one group. Furthermore, using the same reference for both groups guarantee that the subject-level networks of the two groups are in the same space and comparable. Note performing sICA on each group, healthy subjects and patients with SZ, separately showed a high level of spatial similarity with the networks obtained from the full dataset. The average and standard deviation of spatial similarity (correlation) for healthy subjects and patients with SZ are (0.91 ± 0.07) and (0.90 ± 0.09) , respectively. After identifying the brain networks, the time courses of individual networks were used to calculate their dCMs (one dCM per window for each brain network).

3.2 | Spatial state evaluation

To evaluate the time-varying information of brain networks, k -means clustering was applied on the dCMs of each network to group them

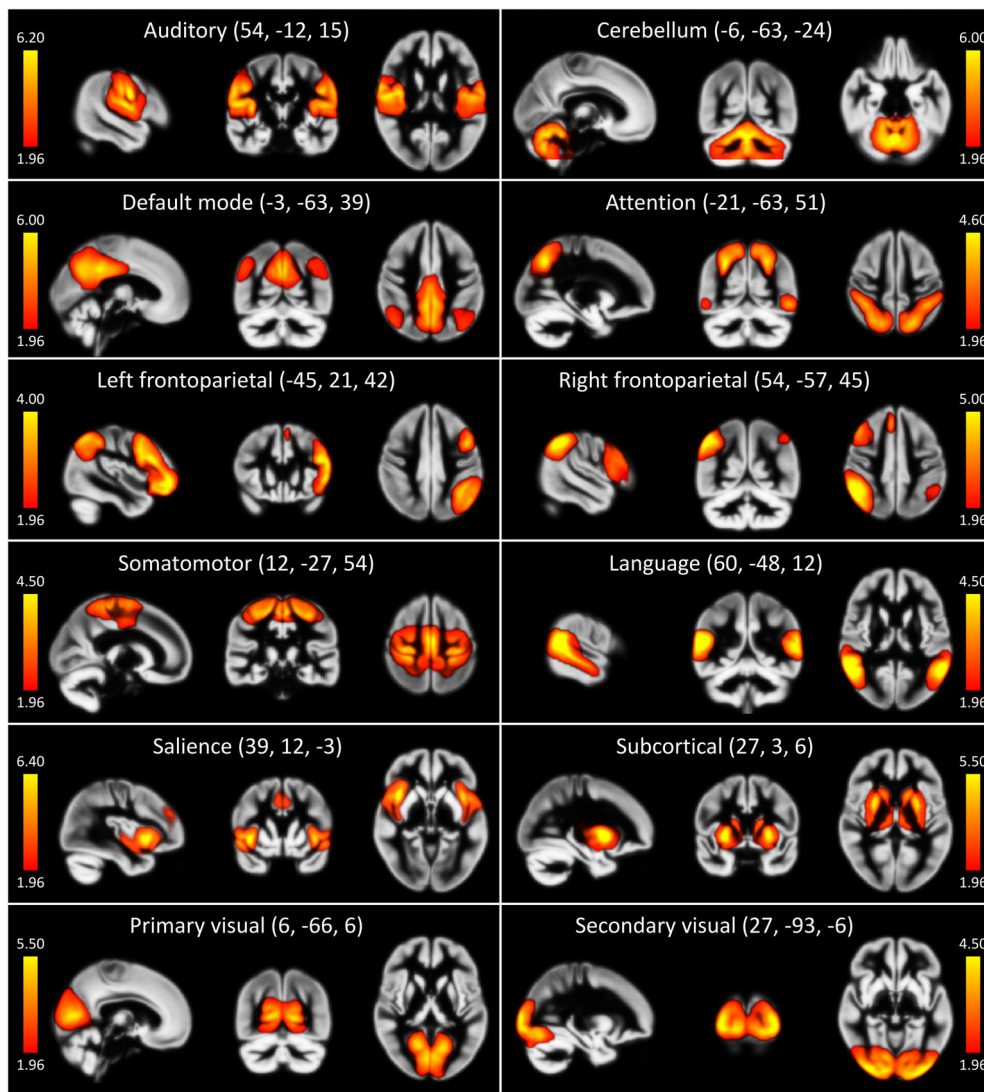


FIGURE 2 Static group spatial functional connectivity maps of the 12 brain networks obtained from spatial independent components analysis. Spatial maps are plotted as z-score and thresholded at $Z > 1.96$ [Color figure can be viewed at wileyonlinelibrary.com]

into a set of distinct spatial patterns called spatial states. This allows us to visualize and quantify the variations in spatial patterns of brain networks. An example of variations in spatial patterns of brain networks and the regions associated with them can be seen in Figure 3, in which three selected spatial states for each brain network represented as red, blue, and green additive color overlays. Regions in white indicate association to a given network in all three states. For instance, the posterior cingulate cortex (PCC) is the central hub of the default mode (Andrews-Hanna, 2012; Leech & Sharp, 2014) and is expected to be part of the default mode all of the time, which is confirmed by being involved in all three states as well as the fourth state, which is not included in Figure 3. However, the thalamus is associated with the default mode in one of the three states (represented in red), and the frontal regions are involved in either one (represented in blue or red) or two states (represented in purple). These findings could explain inconsistencies in previous findings regarding the membership of certain regions to brain networks. For instance, different spatial patterns for the default mode have been observed within the literature (Andrews-Hanna, Reidler, Sepulcre, Poulin, & Buckner, 2010;

Braga & Buckner, 2017; Fox et al., 2005). While most of the original studies did not report the thalamus as part of the default mode (Buckner, Andrews-Hanna, & Schacter, 2008; Fox et al., 2005; Greicius, Krasnow, Reiss, & Menon, 2003), recent studies have shown conflicting results (Lee & Xue, 2018; Shirer, Ryali, Rykhlevskaia, Menon, & Greicius, 2012; Wang et al., 2014). Moreover, different parts of the frontal and prefrontal lobes have been reported as part of the default mode across studies (Braga & Buckner, 2017; Buckner et al., 2008; Damoiseaux et al., 2006; Garrity et al., 2007; Shirer et al., 2012). Similarly, different patterns of regional memberships have been observed across other brain networks (Braga & Buckner, 2017; Damoiseaux et al., 2006; Zuo et al., 2010). Therefore, we suggest that different regions are associated with brain networks at different time points, and only overall patterns of brain networks during data acquisition are identified in the static analysis.

3.2.1 | Anticorrelated brain networks

Evaluating the spatial chronnectome using dCMs also provides new information relating to anticorrelated brain networks (negative



FIGURE 3 RGB additive color-code presentation of three arbitrarily-selected spatial states for brain networks. Red, blue, and green represent the strength of three spatial states. Thus, for instance, white represents the areas in which the brain network is strong in all three spatial states, and yellow shows strong association in red and green spatial states. It is worth mentioning that the spatial states of different brain networks were identified independently; therefore, for example, the first spatial state of network_i is not correspondent with the first spatial state of network_j ($i \neq j$) [Color figure can be viewed at wileyonlinelibrary.com]

associations between brain networks). Previous static studies have observed negative associations between brain networks and their associated regions (Allen et al., 2011; Fox et al., 2005; Fox, Zhang,

Snyder, & Raichle, 2009; Uddin, Kelly, Biswal, Castellanos, & Milham, 2009). For instance, regions of different brain networks (including salience and sensorimotor) are suggested to be negatively correlated

with the default mode regions (Allen et al., 2011; Fox et al., 2005, 2009; Uddin et al., 2009). Our analysis reveals that different, anti-correlated patterns occur at different moments in time. For example, each of the previously reported networks and its associated regions become negatively associated with the default mode for a specific spatial state, and there are moments in which no negative associations exist (Figure 4). In other words, anticorrelative relationships identified across previous default mode static analyses all exist, but in differing segments of time. We further observed new anticorrelated patterns across different networks, including the left and right frontoparietal, salience, somatomotor, and secondary visual networks (Supporting Information S3). This finding emphasizes the importance of time-varying properties that may not be fully captured during static analyses.

3.2.2 | Cerebellar contribution

Despite the important role of the cerebellum, it is often overlooked in brain network analysis. One reason is that the cerebellum is not usually recognized as an integral part of the connectome, with some exceptions, across studies using static analyses. Our analysis reveals

significant contributions of the cerebellum to multiple brain networks, but these contributions are not constant over time (see Figure 3). Different patterns of cerebellar contribution emerge at particular timepoints or states. This highlights a challenge in detecting the role of the cerebellum in brain networks in static analysis. Overall, two major patterns are (a) primarily negative associations between cerebellar regions with sensorimotor networks (e.g., including somatomotor, auditory, and visual networks) and (b) positive associations of cerebellar regions with the subcortical and left and right frontoparietal networks.

3.2.3 | Brain networks are not isolated

Studying spatial chronnectome through spatial states supports the proposition that brain networks are not isolated, and there is strong cross talk between “isolated” brain networks. Spatial chronnectome suggests that regions assigned to one network using static analysis are also involved with other networks at particular points in time. This is observed across all networks but is more dominant in sensorimotor networks, including visual, somatomotor, and auditory networks (Figure 3). The finding that brain networks sometimes merge, or inter-network coupling increases, are consistent with a dynamic interplay between segregation and integration.

3.2.4 | Statistical comparison

The dCMs of brain networks were compared between healthy subjects and patients with SZ. We initially hypothesized networks' dCMs would allow identify nuanced alterations in brain networks in patients with SZ relative to healthy subjects which would not be present in static analyses. This hypothesis was evaluated first by comparing the results of voxel-wise comparisons using spatial states (obtained by applying *k*-means clustering on the dCMs of each brain network) and static connectivity maps (static spatial maps of networks obtained by applying sICA). The results of voxel-wise comparisons are presented in Figure 5a. Both static and spatial state approaches reveal group differences in the cerebellar, subcortical, language, and salience networks. The pattern of differences in these networks is similar between static and spatial states analyses. Static comparison revealed lower static functional connectivity in patients with SZ compared to healthy subjects across these networks except for the putamen in the subcortical network. Similarly, spatial states analyses detected decreases in dynamic couplings across the same networks with the same exception in the subcortical network. In contrast, different and larger regions within networks were found to be altered in patients with SZ compared to healthy subjects in the spatial state analysis compared to the static analysis. Additionally, spatial state analysis shows similar patterns of differences between patients with SZ and healthy subjects in the auditory, primary and secondary visual, somatomotor, default mode, (dorsal) attention, and left frontoparietal networks (Figure 5a). The similarity between static and state analysis patterns further supports the idea that alterations observed in state analysis driven by group differences between patients and healthy subjects. This suggests our spatial state analyses can detect nuanced alterations within patient groups absent in static analyses. For instance, an alteration in a small region of the primary visual network

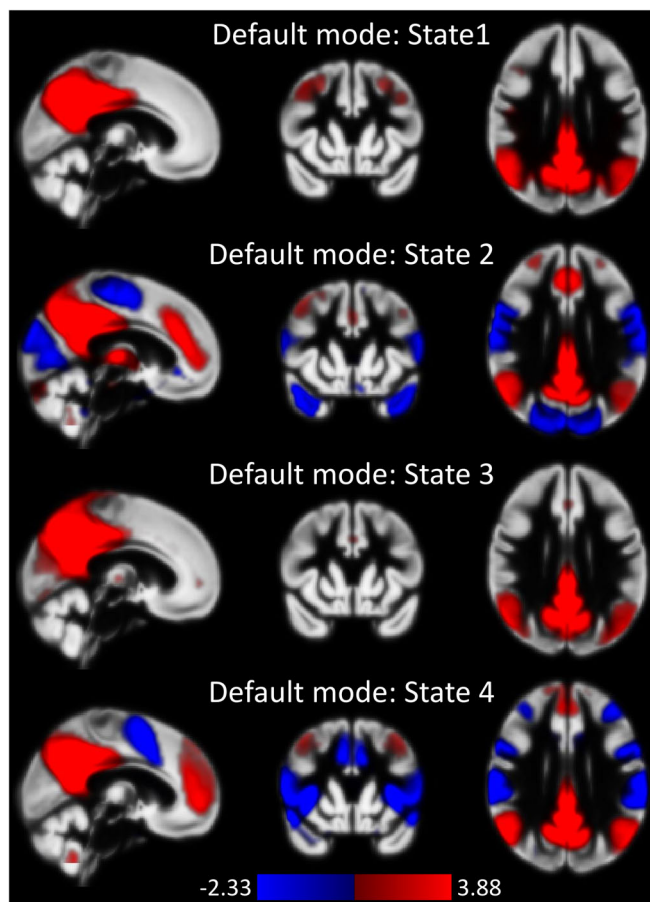


FIGURE 4 The spatial states of the default mode. Hot and cold colors represent positive and negative associations to the default mode, respectively. The results show that sensorimotor areas are anti-correlated with the default mode during State 2, and the salience network is anti-correlated with the default mode during State 4. Importantly, States 1 and 3 do not exhibit an anticorrelative relationship with the default mode [Color figure can be viewed at wileyonlinelibrary.com]

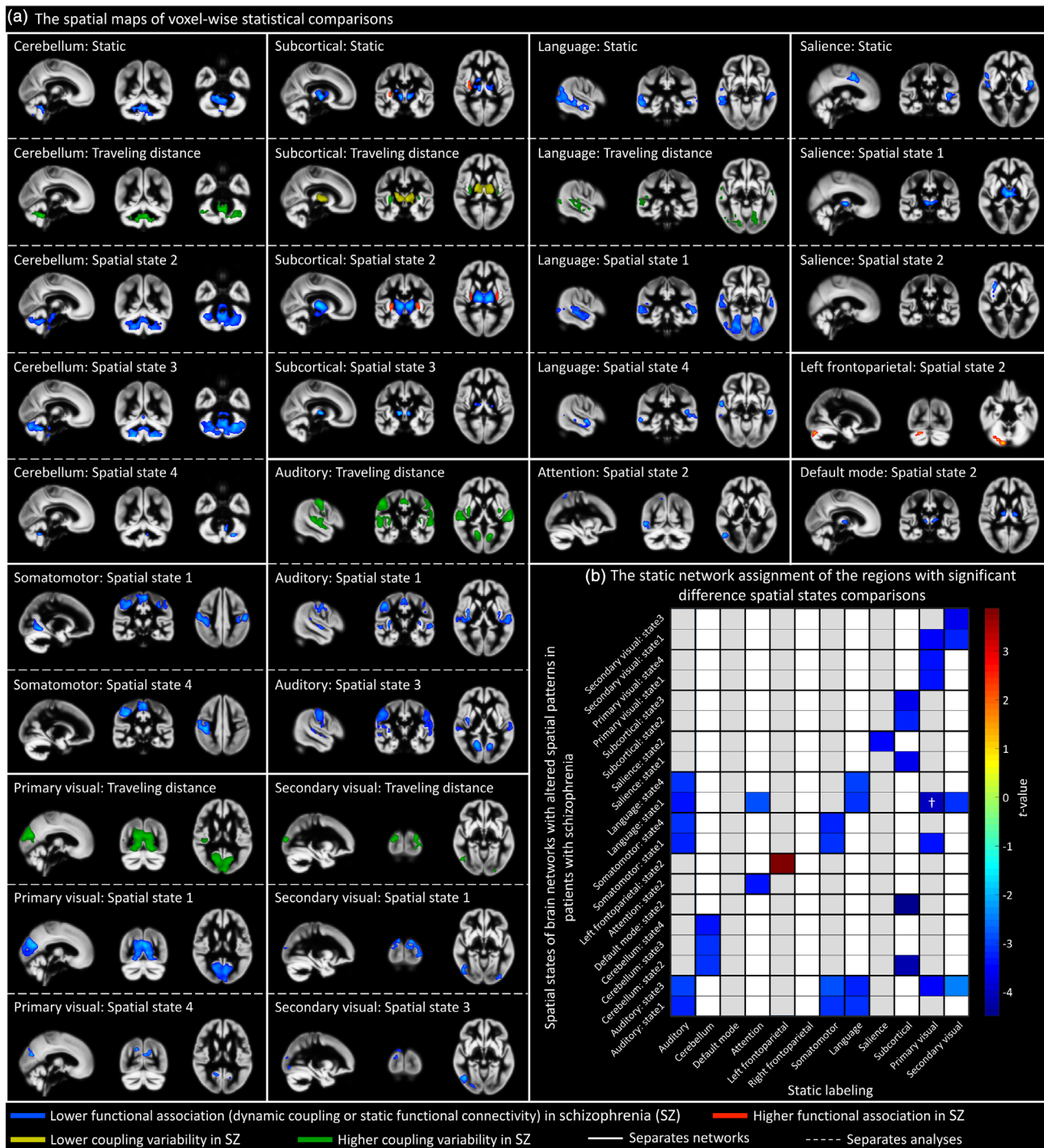


FIGURE 5 Voxel-wise statistical comparisons between healthy subjects and patients with schizophrenia (SZ). Each of the analyses, that is, static, spatial states, and traveling distance (coupling variability), were separately corrected for multiple comparisons using a %5 FDR (Benjamini & Hochberg, 1995). For instance, spatial states were corrected for the total number of comparisons that were performed in spatial states analysis. Only comparisons that show significant differences after FDR corrections are presented here. (a) Spatial maps displaying significant differences between healthy subjects and patients with SZ. Blue and red colors represent lower and higher associations of regions to the networks in patients with SZ relative to healthy subjects, respectively. Yellow and green colors indicate lower and higher coupling variability, that is, variation over time measured by the L1 norm distance, in patients relative to healthy subjects. Networks are separated with solid white colors, while different types of analyses including static functional connectivity, coupling variability (L1 norm distance), and spatial states are separated by dashed white color lines. (b) Summary of voxel-wise comparisons of spatial states. The t-values indicate the degree of statistical differences between patients with SZ vs. healthy subjects. Cold and hot colors show decreased and increased association (network coupling) in patients with SZ relative to healthy subjects, respectively. The Y-axis includes the list of the spatial states of the networks with significant differences between the two groups. The regions that show significant differences in a given spatial state were identified to be part of (i.e., assigned to) different brain networks in static analysis. The X-axis indicates the static network labeling of the regions that show significant differences in state analysis. For instance, the cell labeled with “+” represents the voxels that show a significant difference with reduced dynamic network coupling in patients with SZ (t-value) in State 1 of the language network (Y-axis). These voxels are assigned to (labeled as) the primary visual network in the static analysis (X-axis) [Color figure can be viewed at wileyonlinelibrary.com]

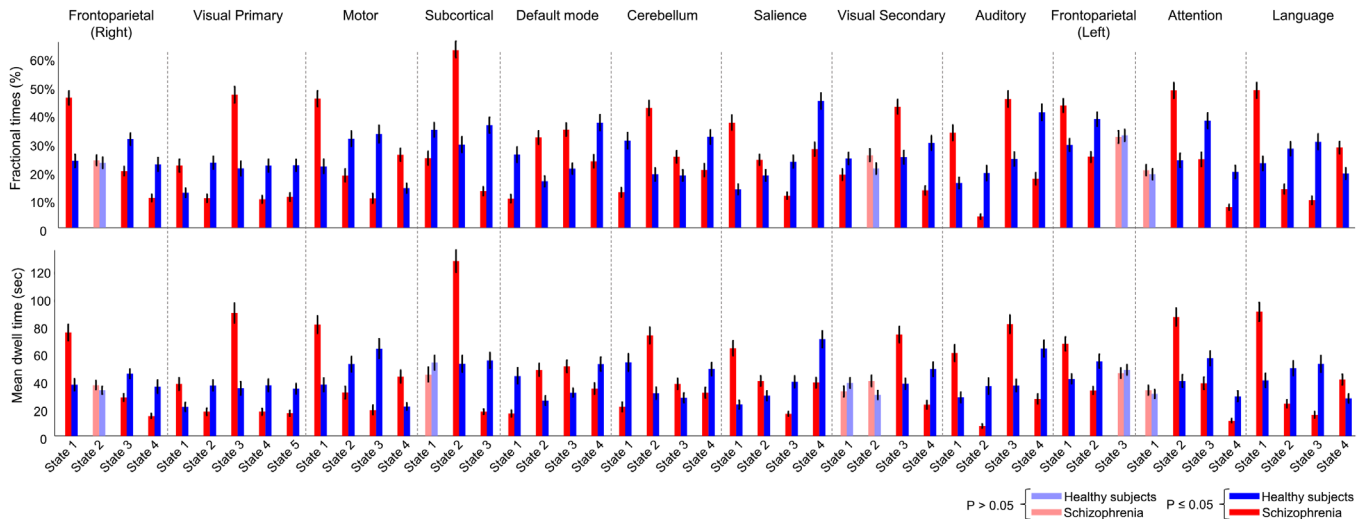


FIGURE 6 The ability of dynamic temporal indices calculated from spatial states to distinguish different cohorts. Two indices including fractional time and mean dwell time were calculated for spatial states of brain networks and compared between healthy subjects and patients with SZ. Statistically significant differences after FDR correction for multiple comparisons were observed between patients with SZ and healthy subjects. The results suggest the ability of the approach to detect patient-based alterations [Color figure can be viewed at wileyonlinelibrary.com]

can also be seen in static analyses if we apply less restrictive criterion that is, using smaller cluster size threshold (Supporting Information S4). Previous studies suggest these networks and associated areas are affected in patients with SZ (Baker et al., 2014; Calhoun, Eichele, & Pearlson, 2009; Garrity et al., 2007; Jafri, Pearlson, Stevens, & Calhoun, 2008; Zeng et al., 2018), which indicates the ability of the approach to both detect known patterns of alterations and also identify novel patterns of patient-based alterations.

It is important to highlight some of the regions within a given network that show differences in the state analysis were not recognized as being part of the same network in the static analysis. In other words, Region w is assigned to the Network j in the static analysis; however, the dynamic analysis reveals that Region w is part of Network i at State k and displays a significant difference between healthy subjects and patients with SZ in State k of Network i . Figure 5b represents a summary of spatial state voxel-wise comparisons and their static labeling. The Y-axis includes the spatial states of the networks illustrating significant differences between healthy subjects and patients with SZ. The X-axis indicates the static network assignment of the regions that show significant differences. For instance, the lingual gyrus is assigned to primary visual network in static analysis, but it is also part of (associated with) the language domain at State 1. This region shows a reduction in its association with State 1 of the language domain in patients with SZ. This emphasizes the advantage of capturing dynamic information about network integration.

While the spatial states of brain networks provide important details of their spatial dynamic, their temporal profiles provide further information regarding the temporal dynamic nature of brain networks. Statistical analyses of mean dwell time and fraction time showed statistically significant differences between patients with SZ and healthy subjects across all networks after FDR correction (Figure 6). In patients with SZ, networks tend to spend more time in spatial states which have high correlations, negative or positive, with sensorimotor regions, particularly within primary visual areas. They include State 1 of the right frontoparietal

network, State 3 of the primary visual network, State 1 of the somatomotor network, State 2 of the subcortical network, State 2 of the default mode network, State 2 of the cerebellar network, State 1 of the saliience network, State 1 of the left frontoparietal network, State 2 of the attention network, and State 1 of the language network.

3.3 | Spatial variation evaluation

3.3.1 | Coupling variability map

Brain networks are spatially fluid, and this spatiotemporal dynamism can be captured and analyzed by calculating coupling variability maps over time. Figure 7 shows variations in the dynamic coupling of associated voxels to a given network over time. Green represents coupling variability, indicating variations in dynamic coupling of each voxel to a given network over time. Red represents static functional connectivity strength. For instance, our results show the PCC that is always associated with the default mode has lower variation over time. However, the thalamus and frontal areas reveal higher variations over time. Evaluating variation in regions' association to brain networks can provide further information about their roles in brain networks. Performing voxel-wise comparisons of coupling variability maps reveal significant differences between healthy subjects and patients with SZ in cerebellar, subcortical, language, auditory, and primary and secondary visual networks (Figure 5a). Thus, we observe higher coupling variability, in addition to lower network coupling strength, among patients with SZ. Collectively, these results suggest both coupling strength and variability are altered in patients with SZ, but the implications of these factors on the SZ phenotype must be explored in future research.

3.3.2 | Spatiotemporal transition matrix

While voxel-wise analysis is important to assess the spatial variations of brain networks, the spatiotemporal transition matrix can quantify and summarize dynamic spatiotemporal properties of individual brain networks. While the variability map captures the overall variations of the functional coupling over time, the spatiotemporal transition matrix

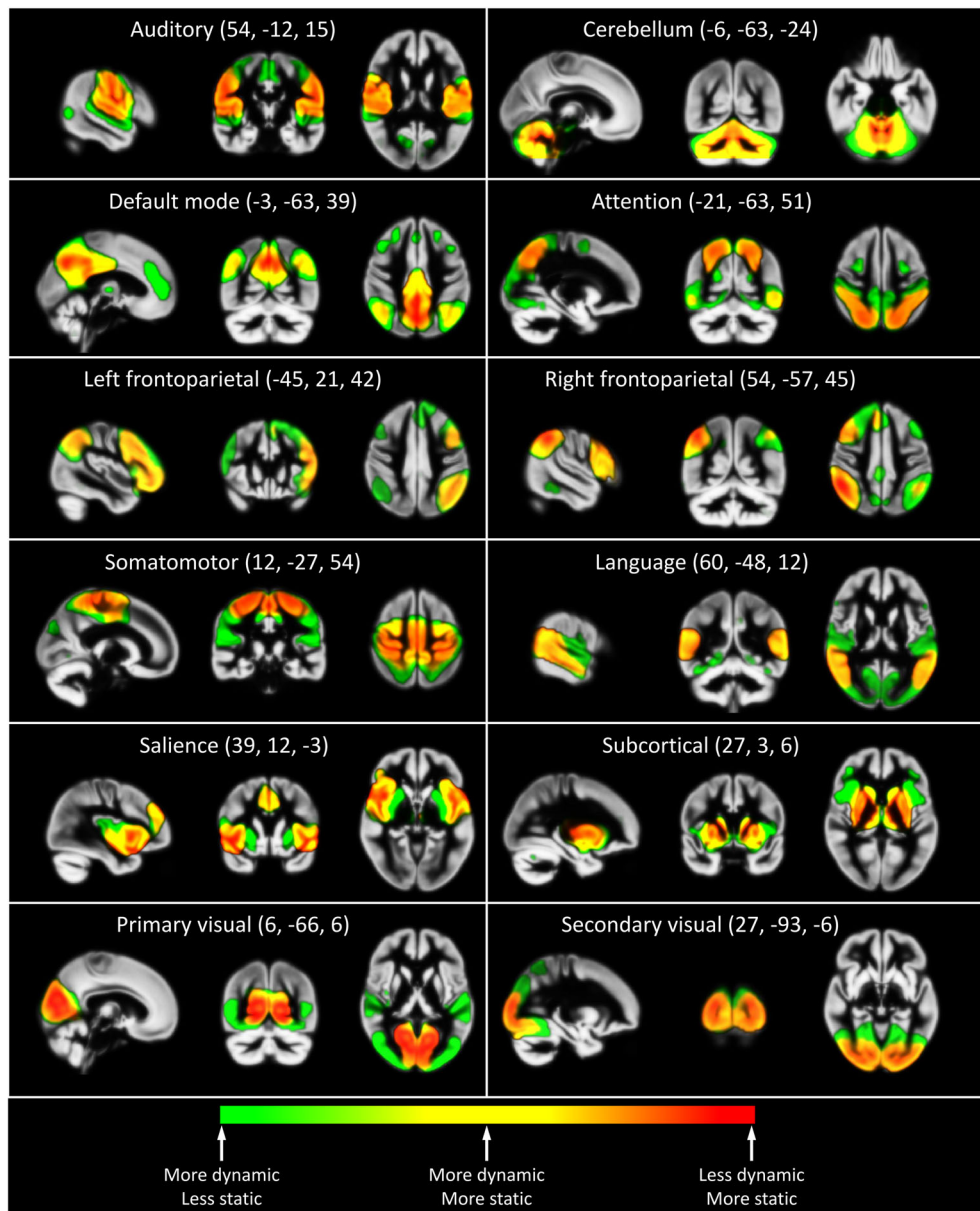


FIGURE 7 Additive color-code representation of networks' coupling variability. Green represents coupling variability estimated by the L1 norm distance of variations in the membership (pairwise correlation) of each voxel to a given network over time. Red represents static functional connectivity strength. Thus, yellow represents the regions with both high coupling variability over time and static strength. The figure indicates extensive variations in spatial patterns of brain networks. Previous work typically ignores levels of variability and the degree to which a voxel contributes to a given network over time, which is captured using this method [Color figure can be viewed at wileyonlinelibrary.com]

provides the details of how these time-varying properties occur. Because of the smoothing effect of the sliding window, the spatiotemporal dynamic properties become easier to distinguish as the interval value increases. However, the pattern of transitions is consistent across interval values (See examples in Supporting Information S5). In Figure 8, we present the findings for the interval value of 30 (the length of the interval = $30 \times TR = 60$ s), which is the amount of transitions between two windows with almost no overlap (Figure 8a). Evaluating the spatiotemporal dynamic properties allows us to detect changes in brain networks such as the default mode which are not detected via a static analyses, as well as in the networks that do show differences in a static analysis. Performing statistical comparisons on the elements of the spatiotemporal transition matrix demonstrate statistically significant differences between healthy

subjects and patients with SZ (Figure 8b). Patients with SZ have higher transitions (greater percentages of transitions between windows) in higher bins, that is, bins with higher dynamic coupling values, and healthy subjects have higher transitions in lower bins (lower dynamic coupling values), with the exception of the default mode, which shows the opposite pattern. Significant differences were observed between healthy subjects and patients with SZ in all networks except the left and right frontoparietal networks. Examples of the comparisons for all possible interval values for multiple networks are included in Supporting Information S6, which display similar patterns for different interval values. The spatiotemporal transition matrix can further be utilized to extract abstract global measures to summarize the dynamic properties of each network. For instance, evaluating spatiotemporal uniformity using the energy index

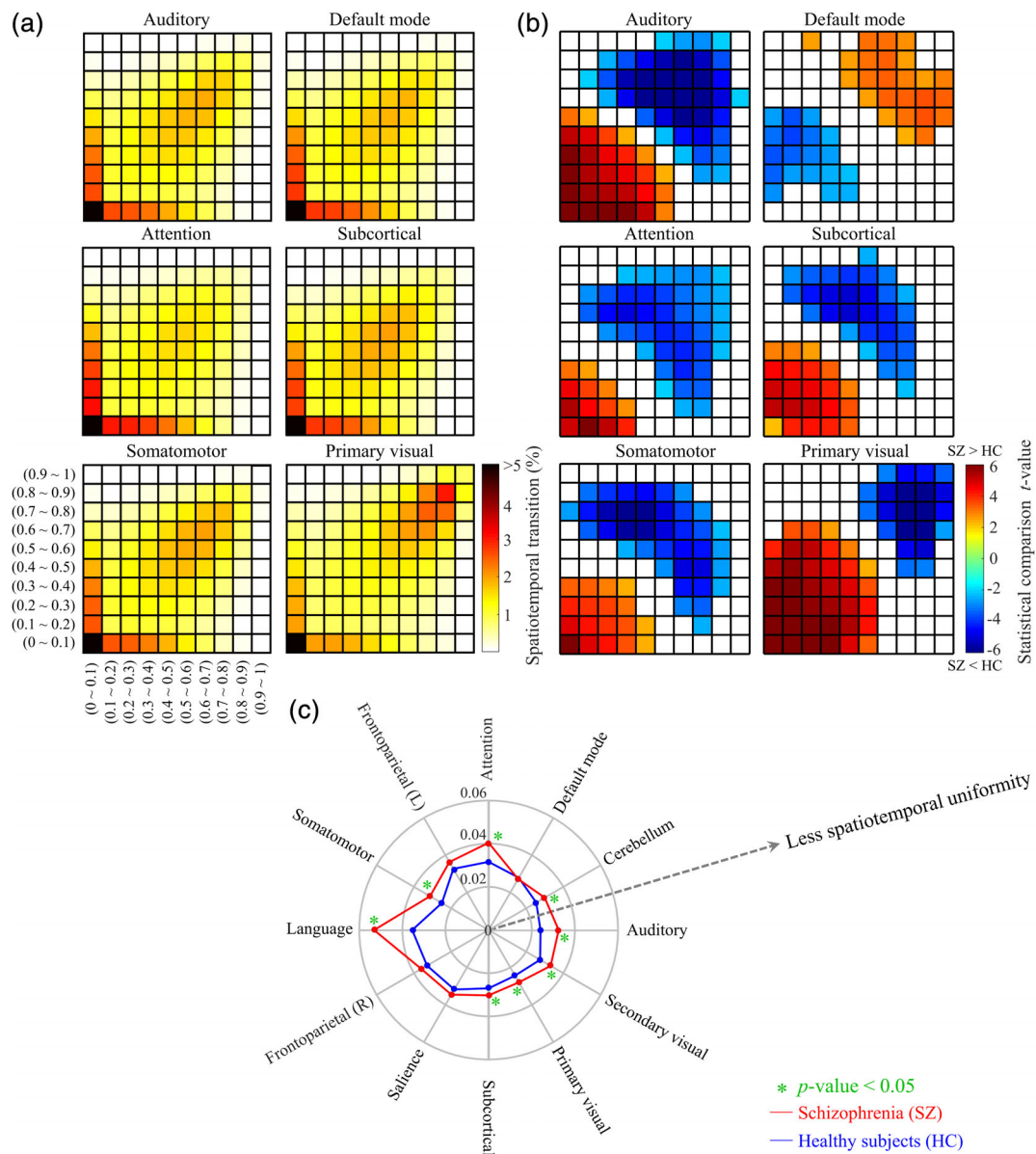


FIGURE 8 Examples of spatiotemporal transition matrices and statistical analysis. (a) The average spatiotemporal transition across all subjects. The spatiotemporal transition matrix for each network summarizes the variation of the network's dCMs (expressed as a correlation between 0 and 1) by discretizing the dynamic coupling values (correlations) into 10 bins. Warm colors represent the percentage of the transition compared to the total number of transitions between every two windows with 60 s distance. For instance, if the number of transitions were uniform, the value of each array would be 1% because there are 100 arrays in the transition matrix. (b) *t*-statistics for group comparisons by diagnosis. Only comparisons which show significant differences after multiple comparison corrections are presented. Blue (cold) and red (hot) colors represent lower and higher transition values in patients with SZ compared to healthy subjects, respectively. (c) Energy index comparison, with greater spatiotemporal uniformity toward the center of the chart. The energy index was measured for the spatiotemporal transition matrix and compared between healthy subjects and patients with SZ. Blue and red colors represent healthy subjects and patients with SZ, respectively. Green asterisks indicate the statistical significant differences between the two groups after multiple comparisons correction using a %5 FDR [Color figure can be viewed at wileyonlinelibrary.com]

shows a significant difference between the two groups, specifically, healthy subjects demonstrated higher spatiotemporal uniformity (i.e., lower energy index) compared to SZ patients (Figure 8c).

Evaluating the relationship between CMINDS and the energy indices displays significant correlations between the energy index of the subcortical domain from the imaging data and attention/vigilance CMINDS domain in the healthy subjects ($\rho = -0.27$; $p < 0.0011$, FDR = 0.049) but not patients with SZ ($\rho = 0.12$; $p < 0.1561$, FDR = 0.962). Furthermore, the group difference of the correlation between

the energy index of the subcortical domain from the imaging data and Attention/Vigilance CMINDS domain approached statistical significance ($p < 0.0012$, FDR = 0.059).

4 | DISCUSSION

Static analysis of fMRI data (i.e., computing correlations based on all timepoints) has provided important information about the brain;

however, the assumption that resting brain activity can be represented by static activity across time is a gross oversimplification which may obscure the true dynamic nature of the brain. The recent findings reveal the ability of fMRI to capture time-varying information about brain connectivity; however, these studies mainly overlook the spatial aspect of brain dynamics. Here, we propose a spatial chronnectome approach which examines the variations in the spatiotemporal coupling of networks at the voxel level. The findings of our study identify spatially fluid behaviors of inter- and intranetwork brain relationships, which have the potential to quantify dynamic interplay between information segregation and integration of functional connections across the brain. Our approach shows that brain networks evolve spatially over time by capturing spatiotemporal variations within brain networks. For instance, our approach identified variability in the brain network membership of a given brain region over time.

For discussion purposes, regions associated with a given brain network can be divided into two categories. The first includes regions which are repeatedly or occasionally reported to be parts of a given network in static analysis. The second category contains brain regions known to be parts of other networks in static analyses based on previous research. Findings related to the first category may explain inconsistent observations regarding the spatial patterns of brain networks. These findings argue that the spatial chronnectome (the temporal variations of the coupling patterns of brain networks) could reflect inconsistencies in the spatial patterns of brain networks and the variability in brain regions' memberships which are obscured in the signal averaging used in static analyses. For example, the thalamus and frontal regions show high variations in their associations to the default mode, even dissociating from the default mode at particular times. The PCC, however, shows a more robust and constant association to the default mode over time, which may reflect its role as the central hub (core) of the default mode. The small amount of variation/variability of the PCC association with the default mode suggests that the cores of brain networks have smaller variations in their dynamic couplings to the associated networks over time. Categorizing regions based on their time-varying associations with brain networks, and evaluating the multifactorial roles and relationship between them may provide new information about the interaction within and between networks.

It is worth mentioning that there is both a high-level of similarity and major differences between the spatial states and the interdigitated networks observed in previous single-subject analysis (Braga & Buckner, 2017) which can be seen, in our opinion, as an alternative interpretation for the observed inconsistency in the spatial patterns of brain networks. The concept of the spatial chronnectome within brain networks does not exclude the existence of a set of parallel networks within each large-scale network, as these also can be identified via brain dynamic analysis. Because a brain region's association to a given large-scale network varies over the time, the associated parallel networks can be captured using the time points during which they contribute to the dominant patterns within the given large-scale networks.

The second category highlights that brain networks are not isolated and exhibit significant cross talk. Regions in different networks join and dissociate from other networks over time. This pattern of integration and segregation occurs across various regions and all investigated networks. These findings reflect an extension of the

classical views of information processing in the brain based on static functional connectivity analyses by providing novel metrics of transient coupling. This approach may have the potential to detect new information about the functional activity of brain regions. For example, the primary visual area, in addition to its role in the visual network, is transiently associated (coupled) with multiple networks which do not typically include visual areas. In our analysis, the primary visual area demonstrates significant positive or negative associations to at least one state of all identified brain networks, suggesting it has a major role in network cross talk. These significant associations may suggest that the primary visual area has significant contribution to brain activities in addition to its role of receiving and delivering visual information from retinal input. There is significant evidence to support the potential role of the primary visual area in other brain functions. While the primary visual area receives most of the retinal input (90%; Sincich, Park, Wohlgenuth, & Horton, 2004), neuronal tracing and neuronal recording investigations demonstrated feedback connections between the primary visual area and many cortical areas (Bullier, Hupe, James, & Girard, 2001; Felleman & Van Essen, 1991; Hupe et al., 2001). For instance, the primary visual area receives information from a wide range of sensory and nonsensory cortices such as the primary auditory, parietal, and frontal cortices (Markov et al., 2011). Moreover, transcranial magnetic stimulation (TMS) interference on the primary visual area introduced impairments to working memory processing (van de Ven, Jacobs, & Sack, 2012). However, the classic view of the primary visual cortex can be well studied by fMRI because fMRI can detect changes associated with higher cognitive function and indirect functional connectivity. fMRI research provides the striking evidence that the primary visual cortex is involved in higher cognitive functions (Bressler, Fortenbaugh, Robertson, & Silver, 2013; Harrison & Tong, 2009; Lars, 2010; Muckli & Petro, 2013; Roelfsema & de Lange, 2016). While our findings are intriguing, it is worth highlighting that they only suggest significant dynamic interplay in temporal coupling measured by the BOLD signal. Further investigation and direct neural activity measurements are needed to establish a concrete understanding of functions for primary visual cortex outside of receiving and delivering visual information from the retinal input. Further validation studies are needed to confirm and extend this work. To conclude, variability in a given region's association to a given brain network highlights a dynamic interplay between segregation and integration, providing a new perspective on the function of well-known brain areas. Our results suggest evaluating time-varying properties of brain network interplay is thus a vital issue for future research to understand the multifactorial role of brain networks.

Studying patterns of brain networks using spatial states also reveals interesting findings regarding anticorrelative patterns of brain networks. Similar to our finding that different brain regions are involved with different brain networks over time, various anticorrelative relationships were detected at different time points. Using a spatial state analysis, the default mode shows anticorrelated relationships with sensorimotor and salience networks at States 2 and 4, respectively, but the anticorrelated pattern attenuates in States 1 and 3. Dynamic anticorrelative patterns for regions associated with the default mode have been previously reported which further support our findings (Chang & Glover, 2010; Yang, Craddock, Margulies,

Yan, & Milham, 2014). Our findings suggest dynamic anticorrelative relationships are not limited to the default mode. We identified a new set of anticorrelated patterns for various networks and illustrate that anticorrelative relationships occur at specific moments rather than persisting over time. This finding suggests the need for new investigations and potential revision to proposed causality or modulatory relationships between brain networks such as between the salience and default mode.

Studying dCMs of brain networks also accentuates the role of the cerebellum in different networks. The cerebellum has widespread polysynaptic connections to the cerebral cortex which all pass through the thalamus (Buckner, Krienen, Castellanos, Diaz, & Yeo, 2011; Kelly & Strick, 2003; Krienen & Buckner, 2009; Strick, Dum, & Fiez, 2009). This phenomenon can explain the role of the cerebellum in a wide range of motor and cognitive functions (Lars, 2010; Muckli & Petro, 2013; Stoodley & Schmahmann, 2009). While the polysynaptic connections make reconstructing the topography of cerebro-cerebellar connections by anatomical methods relatively difficult, functional connectivity is an indirect effective way to map cerebro-cerebellar connections (Krienen & Buckner, 2009; O'Reilly, Beckmann, Tomassini, Ramnani, & Johansen-Berg, 2010). Our observations, similar to previous fMRI studies, demonstrate stronger contralateral connectivity patterns between the cerebellum and cerebral cortex compared to ipsilateral connectivity patterns, which is consistent with known contralateral polysynaptic connections between the cerebral cortex and the cerebellum (Buckner et al., 2011; Kelly & Strick, 2003; Krienen & Buckner, 2009; O'Reilly et al., 2010). In general, previous rsfMRI studies agree on the relationship of the cerebellum with the thalamus, motor area, and regions associated with the frontoparietal networks (Krienen & Buckner, 2009; O'Reilly et al., 2010). Our dynamic network analysis corroborates these results.

Despite the unique ability of rsfMRI to measure cerebro-cerebellar connectivity, the role of the cerebellum in brain network analysis is often overlooked. This is in part because it is not usually recognized as an integral part of the connectome, and its static functional connectivity to brain networks is typically weaker compared to cortical connectivity limiting the visibility of the cerebellum due to limitations in statistical power. In earlier work, Buckner and his colleagues estimated specific cerebellar topography patterns for cerebral networks by assigning each cerebellar voxel to a network with the highest correlation values (Buckner et al., 2011). Although their approach had limitations preventing concrete conclusions, their work provides a striking result regarding different functional connectivity patterns across the cerebellum. Using a dynamic analysis, our findings suggest the evaluation of time-varying contributions of cerebellar regions to different brain networks conjointly can provide a great deal of knowledge about the role of the cerebellum in functional networks. Our analysis showed positive associations between cerebellar regions and the subcortical network, which may be explained by the relay role of the thalamus in cerebro-cerebellar connections. We also observed positive associations between cerebellar regions and both the left and right frontoparietal networks that relate to fronto-cerebellar circuitry (Kelly & Strick, 2003; Krienen & Buckner, 2009; O'Reilly et al., 2010). For the first time, we observe negative associations between cerebellar regions and certain sensorimotor networks. These include

somatomotor, auditory, and visual networks. This negative association could be related to modulating the connection between the thalamus and cortex in cerebellar thalamic cortical circuits.

It is also worth mentioning that functional relationship between the cerebellum and somatosensory and motor/premotor cortex has been frequently reported, but there is some disagreement over the relationship between the cerebellum and both the primary auditory and visual cortices (Krienen & Buckner, 2009; O'Reilly et al., 2010). O'Reilly et al. (2010) suggested the relationship between the cerebellum and primary auditory and visual areas probably reflects the importance of visual and auditory information in motor control which was demonstrated in earlier experiments. Interestingly, the motor area is positively associated with the states of the primary visual and auditory networks that have a negative association with the cerebellum. This also emphasizes the importance of our finding that different networks have cross talk.

While the goal of this work is to introduce an approach to measure the spatial chronnectome, we also evaluate the diagnostic utility of spatial chronnectome by examining the ability of several spatial chronnectome features to differentiate between healthy subjects and patients with SZ. For this purpose, statistical comparisons were performed, and results were corrected for multiple comparisons. To have a fair assessment of each feature's ability to distinguish between two groups, a 5% FDR correction (Benjamini & Hochberg, 1995) was applied based on the total number of the comparisons performed for each feature. Results demonstrate similar patterns of alterations for static and spatial chronnectome analyses, but the spatial chronnectome analyses can capture statistically significant alterations within patient groups missed by a static analyses. Furthermore, the results highlight that the significant differences between healthy controls and patients with SZ are highly similar and consistent across spatial chronnectome features, further supporting the observed findings. Our results are also consistent with and extend findings from previous studies (Baker et al., 2014; Calhoun et al., 2009; Damaraju et al., 2014; Erdeniz, Serin, Ibadı, & Tas, 2017; Garrity et al., 2007; Gavrilescu et al., 2010; Jafri et al., 2008; Skudlarski et al., 2010; Vercammen, Knegeter, den Boer, Liemburg, & Aleman, 2010; Zeng et al., 2018).

Our approach emphasizes distinct features in both the spatial and temporal realms. Regarding spatial patterns of brain networks, the spatial chronnectome procedure allows us to detect atypical brain patterns in patients with SZ which are not detected with a static analysis including statistical alteration in dCMs. Moreover, spatial chronnectome analyses detect important variations in temporally fluid patterns. With respect to temporal dynamic properties, preliminary investigations reveal significant differences in both mean dwell time and fraction time between patients with SZ and healthy subjects. Additional independent studies will be needed to comprehensively investigate the temporal properties of brain networks through networks' state and meta-state indices. Furthermore, our approach provides a unique opportunity to investigate the variations of networks' couplings which is not feasible in static analysis. In general, we observe higher coupling variability and lower network coupling strengths among patients with SZ. This is aligned with the dysconnectivity or disconnection hypothesis of SZ (Friston, 1998). Reduced functional connectivity has been consistently reported in patients with SZ (Damaraju et al., 2014; Erdeniz et al., 2017;

Gavrilescu et al., 2010; Skudlarski et al., 2010; Vercammen et al., 2010), and higher fluctuations of brain connectivity within brain networks in SZ could be related to the brain's effort to compensate for dysconnectivity and/or unbalancing of brain circuitries (Cazorla, Kang, & Kellendonk, 2015).

While the proposed approach can capture the spatial fluidity of networks' couplings, new indices are also needed to quantify the spatiotemporal patterns of individual brain networks. For this purpose, the spatiotemporal transition matrix and associated features were introduced to summarize the time-varying properties. Statistical comparisons between healthy subjects and patients with SZ reveal statistically significant differences which were consistent across interval values. With the exception of the default mode, the patterns of alterations are similar across networks in which patients with SZ have higher transitions in higher dynamic coupling values, while healthy subjects display higher transitions in lower dynamic coupling values. The opposite pattern found in the default mode could be related to its activity pattern in relation to other networks and mental and physical activities. It is known that static functional connectivity within the default mode decreases as the static functional connectivity of the other networks increases. For instance, during a task, the connectivity value within the default mode reduces. Thus, it is expected that variations in lower dynamic coupling values of the default mode are associated with variations in higher dynamic coupling of other networks. Significant differences between healthy subjects and patients with SZ were also observed in networks' spatiotemporal uniformity. Future work should also examine how spatiotemporal dynamic information can improve classification accuracy of patients into diagnostic categories. More importantly, significant associations were detected between spatiotemporal uniformity indices obtained from the spatiotemporal transition matrix and attention/vigilance cognitive domains of CMINDS. Previously, van Erp et al. (2015), found patients with SZ display significantly large impairments in the speed of processing and the attention/vigilance of CMINDS compared to healthy subjects, more so than other CMINDS domains. As such, our findings that there is a strong difference in the links between subcortical and CMINDS attention/vigilance domain may reflect a true disruption in subcortical domains relative to attention/vigilance in patients with SZ, but lack the statistical power for confirmation. Future work is needed to identify the nature of the relationship between spatiotemporal indices and neuropsychological variables in both SZ and other patient groups, but our preliminary results demonstrate promising relationships between the spatial chronnectome metrics and cognitive scores.

4.1 | Limitations and future directions

In this study, we selected specific values for different steps of the proposed pipeline based on existing knowledge from previous studies; although there are many possible avenues for the pipeline. For instance, the proposed approach uses a sliding-window size of 60 s to follow recommendations from previous research, which suggests that data lengths between 30 and 60 s is a good choice to successfully capture dynamic properties (Allen et al., 2014; Preti et al., 2017) and estimate cognitive states (Shirer et al., 2012). The impact of various window lengths on spatially dynamic properties should be evaluated

in future studies. Furthermore, while the sliding-window approach (Allen et al., 2014; Damaraju et al., 2014; Sakoglu et al., 2010) is the most commonly used approach to study time-varying properties of brain networks, we highlight the importance of capturing the dynamic information of BOLD signals to its full potential, that is, up to the maximum frequency that exists in the data (Trapp et al., 2018; Vidaurre et al., 2017; Yaesoubi et al., 2018). Therefore, the approach should be improved to capture the full amount of time-varying information in the data. The other drawback of this work is the spatial resolution of the data, which limits the spatially dynamic specificity. The spatial resolution has a more severe impact when brain regions with very distinct functional roles, like sub-regions of the cerebellum, are located in close proximity to one another. We applied a minimum level of spatial smoothing, that is, FWHM smaller than the width of two voxels, to preserve spatial specificity while reducing the effect of noise; however, data with higher spatial and temporal resolutions can provide better insight into spatiotemporal variations of brain functional organizations. The use of surface-based registrations for high spatial resolution data instead of volume-based registration could potentially enhance functional specialization on the cortex.

In this study, we investigated the spatiotemporal variations of the brain networks, that is, spatially independent functional organizations; however, another set of functional organizations can be obtained by assuming temporal dependency (Calhoun, Adali, Pearson, & Pekar, 2001b; Smith et al., 2012). Temporal independence may be better suited for the proposed approach, as it does not assume spatial stationarity in the first step of the analysis. In other words, using spatially independent networks carries the same contradictory assumption regarding the spatial maps as spatio-temporal (dual) regression analysis (Erhardt et al., 2011). Thus, future studies with higher temporal resolution should be used to investigate the spatial chronnectome of temporally independent networks. Finally, the proposed approach is the first step toward enhancing our understanding of spatiotemporal variations of brain functional organizations at the voxel level. Further work is necessarily to continue to validate and extend this work to investigate the spatial chronnectome of functional organizations across different cohorts (e.g., patients and healthy subjects).

It should be highlighted that our intriguing findings and new discoveries related to brain functional connectivity were only achieved because our approach utilizes the spatial properties of brain dynamics. While most dynamic literature uses fixed spatial nodes/network and ignore the possibility of spatial variations and reconfigurations over time, our approach provides space/time-varying information of individual brain networks at the voxel level. As a result, we were able to observe new information which is invisible to previous dynamic analysis approaches. For instance, our findings demonstrate that time-varying properties are not similar across regions of a given network, and this can only be detected if we utilize spatial dynamic properties. The spatial dynamics also allow us to see how brain regions change their contributions to different networks over time and provide the spatially fluid perspective of functional connectivity variations over time. In short, our approach allows every voxel to present its dynamic properties rather than being limited to the overall dynamic properties of the predefined spatial node that it was assigned to. This is particularly important to properly capture dynamic interplay between

functional segregation and integration. Our proposed approach also allows measuring the simultaneous contributions of each brain region to several networks at any given time, which contrasts to previous dynamic works that assign each region to one network at any given time point or across the entire time series. In other words, our approach is not limited by a priori assumption of regional associations to networks. Another direct benefit of utilizing spatial information is identifying the exact location (regions) of the alterations. For instance, Damaraju et al. (2014) identified similar patterns of alterations in patients with SZ using whole brain dynamic temporal coupling among ICNs. However, they were unable to identify the exact locations of the regions that contribute to those alterations because they did not take advantage of spatial information. On the other hand, our approach allows us to identify the disrupted regions associated with each brain network. Interestingly, many of the atypical regions would not be detected if we used prior knowledge to assign regions to networks.

5 | CONCLUSION

The proposed approach provides a new framework to study the spatial chronnectome of brain functional organizations. Despite the limitations of our analysis/acquisition approach, such as spatial and temporal resolutions and sliding window restrictions, the findings suggest spatiotemporal variations are present within brain networks. Major findings of the study are (a) highlighting spatially fluid behavior of intra- and internetwork relationships, underlying a dynamic interplay between segregation and integration of information; (b) providing a potential explanation for a broad-spectrum of inconsistencies in findings of static functional connectivity analyses; and (c) extracting detailed information and nuanced alterations of brain networks which would not be possible with a static analysis. Furthermore, new indices are introduced to evaluate spatiotemporal variations in brain functional organizations such as brain networks. Preliminary assessments of the approach using healthy subjects and patients with SZ demonstrate the approach may be able to obtain novel information of brain function and detect alterations among patients with SZ. Further investigation should evaluate the ability and validity of using the spatial chronnectome to study spatiotemporal variations of brain functional organizations.

ACKNOWLEDGMENTS

This work was supported by grants from the National Institutes of Health grant numbers 2R01EB005846, R01REB020407, and P20GM103472; and National Science Foundation (NSF) grant 1539067 to Dr. Vince Calhoun. The authors thank Srinivas Rachakonda and Eswar Damaraju for their input.

ORCID

Armin Irajji  <https://orcid.org/0000-0002-0605-593X>

Maziar Yaesoubi  <https://orcid.org/0000-0002-5186-5683>

REFERENCES

- Allen, E. A., Damaraju, E., Plis, S. M., Erhardt, E. B., Eichele, T., & Calhoun, V. D. (2014). Tracking whole-brain connectivity dynamics in the resting state. *Cerebral Cortex*, *24*, 663–676.
- Allen, E. A., Erhardt, E. B., Damaraju, E., Gruner, W., Segall, J. M., Silva, R. F., ... Calhoun, V. D. (2011). A baseline for the multivariate comparison of resting-state networks. *Frontiers in Systems Neuroscience*, *5*, 2.
- Andrews-Hanna, J. R. (2012). The brain's default network and its adaptive role in internal mentation. *The Neuroscientist*, *18*, 251–270.
- Andrews-Hanna, J. R., Reidler, J. S., Sepulcre, J., Poulin, R., & Buckner, R. L. (2010). Functional-anatomic fractionation of the brain's default network. *Neuron*, *65*, 550–562.
- Arbabshirani, M. R., Plis, S., Sui, J., & Calhoun, V. D. (2017). Single subject prediction of brain disorders in neuroimaging: Promises and pitfalls. *NeuroImage*, *145*, 137–165.
- Arthur, D., Vassilvitskii, S., 2007. k-means++: The advantages of careful seeding. *Proceedings of the eighteenth annual ACM-SIAM symposium on Discrete algorithms*. Society for Industrial and Applied Mathematics. pp. 1027–1035.
- Baker, J. T., Holmes, A. J., Masters, G. A., Yeo, B. T., Krienen, F., Buckner, R. L., & Ongur, D. (2014). Disruption of cortical association networks in schizophrenia and psychotic bipolar disorder. *JAMA Psychiatry*, *71*, 109–118.
- Barttfeld, P., Uhrig, L., Sitt, J. D., Sigman, M., Jarraya, B., & Dehaene, S. (2015). Signature of consciousness in the dynamics of resting-state brain activity. *Proceedings of the National Academy of Sciences of the United States of America*, *112*, 887–892.
- Beckmann, C. F., DeLuca, M., Devlin, J. T., & Smith, S. M. (2005). Investigations into resting-state connectivity using independent component analysis. *Philosophical Transactions of the Royal Society of London. Series B, Biological Sciences*, *360*, 1001–1013.
- Bell, A. J., & Sejnowski, T. J. (1995). An information-maximization approach to blind separation and blind deconvolution. *Neural Computation*, *7*, 1129–1159.
- Benjamini, Y., & Hochberg, Y. (1995). Controlling the false discovery rate: A practical and powerful approach to multiple testing. *Journal of the Royal Statistical Society. Series B (Methodological)*, *57*, 289–300.
- Biswal, B. B., Mennes, M., Zuo, X. N., Gohel, S., Kelly, C., Smith, S. M., ... Milham, M. P. (2010). Toward discovery science of human brain function. *Proceedings of the National Academy of Sciences of the United States of America*, *107*, 4734–4739.
- Braga, R. M., & Buckner, R. L. (2017). Parallel interdigitated distributed networks within the individual estimated by intrinsic functional connectivity. *Neuron*, *95*, 457–471.
- Bressler, D. W., Fortenbaugh, F. C., Robertson, L. C., & Silver, M. A. (2013). Visual spatial attention enhances the amplitude of positive and negative fMRI responses to visual stimulation in an eccentricity-dependent manner. *Vision Research*, *85*, 104–112.
- Buckner, R. L., Andrews-Hanna, J. R., & Schacter, D. L. (2008). The brain's default network: Anatomy, function, and relevance to disease. *Annals of the New York Academy of Sciences*, *1124*, 1–38.
- Buckner, R. L., Krienen, F. M., Castellanos, A., Diaz, J. C., & Yeo, B. T. (2011). The organization of the human cerebellum estimated by intrinsic functional connectivity. *Journal of Neurophysiology*, *106*, 2322–2345.
- Buckner, R. L., Sepulcre, J., Talukdar, T., Krienen, F. M., Liu, H., Hedden, T., ... Johnson, K. A. (2009). Cortical hubs revealed by intrinsic functional connectivity: Mapping, assessment of stability, and relation to Alzheimer's disease. *The Journal of Neuroscience*, *29*, 1860–1873.
- Bullier, J., Hupe, J. M., James, A. C., & Girard, P. (2001). The role of feedback connections in shaping the responses of visual cortical neurons. *Progress in Brain Research*, *134*, 193–204.
- Calhoun, V. D., & Adali, T. (2012). Multisubject independent component analysis of fMRI: A decade of intrinsic networks, default mode, and neurodiagnostic discovery. *IEEE Reviews in Biomedical Engineering*, *5*, 60–73.
- Calhoun, V. D., Adali, T., Pearson, G. D., & Pekar, J. J. (2001a). A method for making group inferences from functional MRI data using independent component analysis. *Human Brain Mapping*, *14*, 140–151.

- Calhoun, V. D., Adali, T., Pearlson, G. D., & Pekar, J. J. (2001b). Spatial and temporal independent component analysis of functional MRI data containing a pair of task-related waveforms. *Human Brain Mapping*, *13*, 43–53.
- Calhoun, V. D., Eichele, T., & Pearlson, G. (2009). Functional brain networks in schizophrenia: A review. *Frontiers in Human Neuroscience*, *3*, 17.
- Calhoun, V. D., Kiehl, K. A., & Pearlson, G. D. (2008). Modulation of temporally coherent brain networks estimated using ICA at rest and during cognitive tasks. *Human Brain Mapping*, *29*, 828–838.
- Calhoun, V. D., Miller, R., Pearlson, G., & Adali, T. (2014). The chronnectome: Time-varying connectivity networks as the next frontier in fMRI data discovery. *Neuron*, *84*, 262–274.
- Cazorla, M., Kang, U. J., & Kellendonk, C. (2015). Balancing the basal ganglia circuitry: A possible new role for dopamine D2 receptors in health and disease. *Movement Disorders*, *30*, 895–903.
- Chang, C., & Glover, G. H. (2010). Time-frequency dynamics of resting-state brain connectivity measured with fMRI. *NeuroImage*, *50*, 81–98.
- Chen, T., Cai, W., Ryali, S., Supekar, K., & Menon, V. (2016). Distinct global brain dynamics and spatiotemporal Organization of the Salience Network. *PLoS Biology*, *14*, e1002469.
- Ciric, R., Nomi, J. S., Uddin, L. Q., & Satpute, A. B. (2017). Contextual connectivity: A framework for understanding the intrinsic dynamic architecture of large-scale functional brain networks. *Scientific Reports*, *7*, 6537.
- Correa, N., Adali, T., & Calhoun, V. D. (2007). Performance of blind source separation algorithms for FMRI analysis using a group ICA method. *Magnetic Resonance Imaging*, *25*, 684–694.
- Correa, N., Adali, T., Li, Y.-O., Calhoun, V.D., 2005. Comparison of blind source separation algorithms for FMRI using a new Matlab toolbox: GIFT. Acoustics, Speech, and Signal Processing, 2005. *Proceedings. (ICASSP'05). IEEE International Conference on IEEE*. Vol. 405, pp. v/401–v/404.
- Damaraju, E., Allen, E. A., Belger, A., Ford, J. M., McEwen, S., Mathalon, D. H., ... Calhoun, V. D. (2014). Dynamic functional connectivity analysis reveals transient states of dysconnectivity in schizophrenia. *NeuroImage: Clinical*, *5*, 298–308.
- Damoiseaux, J. S., Rombouts, S. A. R. B., Barkhof, F., Scheltens, P., Stam, C. J., Smith, S. M., & Beckmann, C. F. (2006). Consistent resting-state networks across healthy subjects. *Proceedings of the National Academy of Sciences of the United States of America*, *103*, 13848–13853.
- Du, Y., & Fan, Y. (2013). Group information guided ICA for fMRI data analysis. *NeuroImage*, *69*, 157–197.
- Du, Y., Pearlson, G. D., Liu, J., Sui, J., Yu, Q., He, H., ... Calhoun, V. D. (2015). A group ICA based framework for evaluating resting fMRI markers when disease categories are unclear: Application to schizophrenia, bipolar, and schizoaffective disorders. *NeuroImage*, *122*, 272–280.
- Erdeniz, B., Serin, E., Ibadi, Y., & Tas, C. (2017). Decreased functional connectivity in schizophrenia: The relationship between social functioning, social cognition and graph theoretical network measures. *Psychiatry Research: Neuroimaging*, *270*, 22–31.
- Erhardt, E. B., Allen, E. A., Damaraju, E., & Calhoun, V. D. (2011). On network derivation, classification, and visualization: A response to Habeck and Moeller. *Brain Connectivity*, *1*, 105–110.
- Erhardt, E. B., Rachakonda, S., Bedrick, E. J., Allen, E. A., Adali, T., & Calhoun, V. D. (2011). Comparison of multi-subject ICA methods for analysis of fMRI data. *Human Brain Mapping*, *32*, 2075–2095.
- Felleman, D. J., & Van Essen, D. C. (1991). Distributed hierarchical processing in the primate cerebral cortex. *Cerebral Cortex*, *1*, 1–47.
- Fox, M. D., Corbetta, M., Snyder, A. Z., Vincent, J. L., & Raichle, M. E. (2006). Spontaneous neuronal activity distinguishes human dorsal and ventral attention systems. *Proceedings of the National Academy of Sciences of the United States of America*, *103*, 10046–10051.
- Fox, M. D., Snyder, A. Z., Vincent, J. L., Corbetta, M., Van Essen, D. C., & Raichle, M. E. (2005). The human brain is intrinsically organized into dynamic, anticorrelated functional networks. *Proceedings of the National Academy of Sciences of the United States of America*, *102*, 9673–9678.
- Fox, M. D., Zhang, D., Snyder, A. Z., & Raichle, M. E. (2009). The global signal and observed anticorrelated resting state brain networks. *Journal of Neurophysiology*, *101*, 3270–3283.
- Franco, A. R., Pritchard, A., Calhoun, V. D., & Mayer, A. R. (2009). Interrater and intermethod reliability of default mode network selection. *Human Brain Mapping*, *30*, 2293–2303.
- Friston, K. J. (1998). The disconnection hypothesis. *Schizophrenia Research*, *30*, 115–125.
- Garrity, A. G., Pearlson, G. D., McKiernan, K., Lloyd, D., Kiehl, K. A., & Calhoun, V. D. (2007). Aberrant "default mode" functional connectivity in schizophrenia. *The American Journal of Psychiatry*, *164*, 450–457.
- Gavrilescu, M., Rossell, S., Stuart, G. W., Shea, T. L., Innes-Brown, H., Henshall, K., ... Egan, G. F. (2010). Reduced connectivity of the auditory cortex in patients with auditory hallucinations: A resting state functional magnetic resonance imaging study. *Psychological Medicine*, *40*, 1149–1158.
- Greicius, M. (2008). Resting-state functional connectivity in neuropsychiatric disorders. *Current Opinion in Neurology*, *21*, 424–430.
- Greicius, M. D., Krasnow, B., Reiss, A. L., & Menon, V. (2003). Functional connectivity in the resting brain: A network analysis of the default mode hypothesis. *Proceedings of the National Academy of Sciences of the United States of America*, *100*, 253–258.
- Guo, C. C., Kurth, F., Zhou, J., Mayer, E. A., Eickhoff, S. B., Kramer, J. H., & Seeley, W. W. (2012). One-year test-retest reliability of intrinsic connectivity network fMRI in older adults. *NeuroImage*, *61*, 1471–1483.
- Haralick, R. M., Shanmugam, K., & Dinstein, I. H. (1973). Textural features for image classification. *IEEE Transactions on Systems, Man, and Cybernetics*, *3*, 610–621.
- Harrison, S. A., & Tong, F. (2009). Decoding reveals the contents of visual working memory in early visual areas. *Nature*, *458*, 632–635.
- Himberg, J., Hyvarinen, A., & Esposito, F. (2004). Validating the independent components of neuroimaging time series via clustering and visualization. *NeuroImage*, *22*, 1214–1222.
- Huqe, J. M., James, A. C., Girard, P., Lomber, S. G., Payne, B. R., & Bullier, J. (2001). Feedback connections act on the early part of the responses in monkey visual cortex. *Journal of Neurophysiology*, *85*, 134–145.
- Hutchison, R. M., Womelsdorf, T., Allen, E. A., Bandettini, P. A., Calhoun, V. D., Corbetta, M., ... Chang, C. (2013). Dynamic functional connectivity: Promise, issues, and interpretations. *NeuroImage*, *80*, 360–378.
- Iraji, A., Benson, R. R., Welch, R. D., O'Neil, B. J., Woodard, J. L., Ayaz, S. I., ... Kou, Z. (2015). Resting state functional connectivity in mild traumatic brain injury at the acute stage: Independent component and seed-based analyses. *Journal of Neurotrauma*, *32*, 1031–1045.
- Iraji, A., Calhoun, V. D., Wiseman, N. M., Davoodi-Bojd, E., Avnaki, M. R. N., Haacke, E. M., & Kou, Z. (2016). The connectivity domain: Analyzing resting state fMRI data using feature-based data-driven and model-based methods. *NeuroImage*, *134*, 494–507.
- Iraji, A., Fu, Z., Damaraju, E., DeRamus, T. P., Lewis, N., Bustillo, J. R., ... Calhoun, V. D. (2018). Spatial dynamics within and between brain functional domains: A hierarchical approach to study time-varying brain function. *Human Brain Mapping*. <http://doi.org/10.1002/hbm.24505>. [Epub ahead of print]
- Jafri, M. J., Pearlson, G. D., Stevens, M., & Calhoun, V. D. (2008). A method for functional network connectivity among spatially independent resting-state components in schizophrenia. *NeuroImage*, *39*, 1666–1681.
- Karahanoglu, F. I., & Van De Ville, D. (2015). Transient brain activity disentangles fMRI resting-state dynamics in terms of spatially and temporally overlapping networks. *Nature Communications*, *6*, 7751.
- Kelly, R. M., & Strick, P. L. (2003). Cerebellar loops with motor cortex and prefrontal cortex of a nonhuman primate. *The Journal of Neuroscience*, *23*, 8432–8444.
- Kiviniemi, V., Vire, T., Remes, J., Elseoud, A. A., Starck, T., Tervonen, O., & Nikkinen, J. (2011). A sliding time-window ICA reveals spatial variability of the default mode network in time. *Brain Connectivity*, *1*, 339–347.
- Krienen, F. M., & Buckner, R. L. (2009). Segregated fronto-cerebellar circuits revealed by intrinsic functional connectivity. *Cerebral Cortex*, *19*, 2485–2497.

- Lars, M. (2010). What are we missing here? Brain imaging evidence for higher cognitive functions in primary visual cortex V1. *International Journal of Imaging Systems and Technology*, 20, 131–139.
- Laumann, T. O., Gordon, E. M., Adeyemo, B., Snyder, A. Z., Joo, S. J., Chen, M. Y., ... Petersen, S. E. (2015). Functional system and areal organization of a Highly Sampled Individual Human Brain. *Neuron*, 87, 657–670.
- Lee, T. W., & Xue, S. W. (2018). Functional connectivity maps based on hippocampal and thalamic dynamics may account for the default-mode network. *The European Journal of Neuroscience*, 47, 388–398.
- Leech, R., & Sharp, D. J. (2014). The role of the posterior cingulate cortex in cognition and disease. *Brain*, 137, 12–32.
- Leonardi, N., Richiardi, J., Gschwind, M., Simioni, S., Annoni, J. M., Schlup, M., ... Van De Ville, D. (2013). Principal components of functional connectivity: A new approach to study dynamic brain connectivity during rest. *NeuroImage*, 83, 937–950.
- Liu, X., & Duyn, J. H. (2013). Time-varying functional network information extracted from brief instances of spontaneous brain activity. *Proceedings of the National Academy of Sciences of the United States of America*, 110, 4392–4397.
- Ma, S., Calhoun, V. D., Phlypo, R., & Adali, T. (2014). Dynamic changes of spatial functional network connectivity in healthy individuals and schizophrenia patients using independent vector analysis. *NeuroImage*, 90, 196–206.
- Ma, S., Correa, N. M., Li, X. L., Eichele, T., Calhoun, V. D., & Adali, T. (2011). Automatic identification of functional clusters in fMRI data using spatial dependence. *IEEE Transactions on Biomedical Engineering*, 58, 3406–3417.
- Markov, N. T., Misery, P., Falchier, A., Lamy, C., Vezoli, J., Quilodran, R., ... Knoblauch, K. (2011). Weight consistency specifies regularities of macaque cortical networks. *Cerebral Cortex*, 21, 1254–1272.
- Menon, V. (2011). Large-scale brain networks and psychopathology: A unifying triple network model. *Trends in Cognitive Sciences*, 15, 483–506.
- Muckli, L., & Petro, L. S. (2013). Network interactions: Non-geniculate input to V1. *Current Opinion in Neurobiology*, 23, 195–201.
- O'Reilly, J. X., Beckmann, C. F., Tomassini, V., Ramnani, N., & Johansen-Berg, H. (2010). Distinct and overlapping functional zones in the cerebellum defined by resting state functional connectivity. *Cerebral Cortex*, 20, 953–965.
- Power, J. D., Barnes, K. A., Snyder, A. Z., Schlaggar, B. L., & Petersen, S. E. (2012). Spurious but systematic correlations in functional connectivity MRI networks arise from subject motion. *NeuroImage*, 59, 2142–2154.
- Preti, M. G., Bolton, T. A., & Van De Ville, D. (2017). The dynamic functional connectome: State-of-the-art and perspectives. *NeuroImage*, 160, 41–54.
- Preti, M. G., & Van De Ville, D. (2017). Dynamics of functional connectivity at high spatial resolution reveal long-range interactions and fine-scale organization. *Scientific Reports*, 7, 12773.
- Roelfsema, P. R., & de Lange, F. P. (2016). Early visual cortex as a multi-scale cognitive blackboard. *Annual Review of Vision Science*, 2, 131–151.
- Sakoglu, U., Pearlson, G. D., Kiehl, K. A., Wang, Y. M., Michael, A. M., & Calhoun, V. D. (2010). A method for evaluating dynamic functional network connectivity and task-modulation: Application to schizophrenia. *Magma*, 23, 351–366.
- Seeley, W. W., Crawford, R. K., Zhou, J., Miller, B. L., & Greicius, M. D. (2009). Neurodegenerative diseases target large-scale human brain networks. *Neuron*, 62, 42–52.
- Shehzad, Z., Kelly, A. M., Reiss, P. T., Gee, D. G., Gotimer, K., Uddin, L. Q., ... Milham, M. P. (2009). The resting brain: Unconstrained yet reliable. *Cerebral Cortex*, 19, 2209–2229.
- Shine, J. M., Koyejo, O., & Poldrack, R. A. (2016). Temporal metastates are associated with differential patterns of time-resolved connectivity, network topology, and attention. *Proceedings of the National Academy of Sciences of the United States of America*, 113, 9888–9891.
- Shirer, W. R., Ryali, S., Rykhlevskaia, E., Menon, V., & Greicius, M. D. (2012). Decoding subject-driven cognitive states with whole-brain connectivity patterns. *Cerebral Cortex*, 22, 158–165.
- Sincich, L. C., Park, K. F., Wohlgenuth, M. J., & Horton, J. C. (2004). Bypassing V1: A direct geniculate input to area MT. *Nature Neuroscience*, 7, 1123–1128.
- Skudlarski, P., Jagannathan, K., Anderson, K., Stevens, M. C., Calhoun, V. D., Skudlarska, B. A., & Pearlson, G. (2010). Brain connectivity is not only lower but different in schizophrenia: A combined anatomical and functional approach. *Biological Psychiatry*, 68, 61–69.
- Smith, S. M., Fox, P. T., Miller, K. L., Glahn, D. C., Fox, P. M., Mackay, C. E., ... Beckmann, C. F. (2009). Correspondence of the brain's functional architecture during activation and rest. *Proceedings of the National Academy of Sciences of the United States of America*, 106, 13040–13045.
- Smith, S. M., Miller, K. L., Moeller, S., Xu, J., Auerbach, E. J., Woolrich, M. W., ... Ugurbil, K. (2012). Temporally-independent functional modes of spontaneous brain activity. *Proceedings of the National Academy of Sciences of the United States of America*, 109, 3131–3136.
- Sorg, C., Riedel, V., Muhlau, M., Calhoun, V. D., Eichele, T., Laer, L., ... Wohlschlagger, A. M. (2007). Selective changes of resting-state networks in individuals at risk for Alzheimer's disease. *Proceedings of the National Academy of Sciences of the United States of America*, 104, 18760–18765.
- Stoodley, C. J., & Schmahmann, J. D. (2009). Functional topography in the human cerebellum: A meta-analysis of neuroimaging studies. *NeuroImage*, 44, 489–501.
- Strick, P. L., Dum, R. P., & Fiez, J. A. (2009). Cerebellum and nonmotor function. *Annual Review of Neuroscience*, 32, 413–434.
- Tagliazucchi, E., Balenzuela, P., Fraiman, D., & Chialvo, D. R. (2012). Criticality in large-scale brain fMRI dynamics unveiled by a novel point process analysis. *Frontiers in Physiology*, 3, 15.
- Trapp, C., Vakamudi, K., & Posse, S. (2018). On the detection of high frequency correlations in resting state fMRI. *NeuroImage*, 164, 202–213.
- Uddin, L. Q., Kelly, A. M., Biswal, B. B., Castellanos, F. X., & Milham, M. P. (2009). Functional connectivity of default mode network components: Correlation, anticorrelation, and causality. *Human Brain Mapping*, 30, 625–637.
- van de Ven, V., Jacobs, C., & Sack, A. T. (2012). Topographic contribution of early visual cortex to short-term memory consolidation: A transcranial magnetic stimulation study. *The Journal of Neuroscience*, 32, 4–11.
- van den Heuvel, M. P., Mandl, R. C., Kahn, R. S., & Hulshoff Pol, H. E. (2009). Functionally linked resting-state networks reflect the underlying structural connectivity architecture of the human brain. *Human Brain Mapping*, 30, 3127–3141.
- Van Dijk, K. R., Hedden, T., Venkataraman, A., Evans, K. C., Lazar, S. W., & Buckner, R. L. (2010). Intrinsic functional connectivity as a tool for human connectomics: Theory, properties, and optimization. *Journal of Neurophysiology*, 103, 297–321.
- van Erp, T. G., Preda, A., Turner, J. A., Callahan, S., Calhoun, V. D., Bustillo, J. R., ... Potkin, S. G. (2015). Neuropsychological profile in adult schizophrenia measured with the CMINDS. *Psychiatry Research*, 230, 826–834.
- Vercammen, A., Knegtering, H., den Boer, J. A., Liemburg, E. J., & Aleman, A. (2010). Auditory hallucinations in schizophrenia are associated with reduced functional connectivity of the temporo-parietal area. *Biological Psychiatry*, 67, 912–918.
- Vidaurre, D., Smith, S. M., & Woolrich, M. W. (2017). Brain network dynamics are hierarchically organized in time. *Proceedings of the National Academy of Sciences of the United States of America*, 114, 12827–12832.
- Wang, X., Xu, M., Song, Y., Li, X., Zhen, Z., Yang, Z., & Liu, J. (2014). The network property of the thalamus in the default mode network is correlated with trait mindfulness. *Neuroscience*, 278, 291–301.
- Yaesoubi, M., Adali, T., & Calhoun, V. D. (2018). A window-less approach for capturing time-varying connectivity in fMRI data reveals the presence of states with variable rates of change. *Human Brain Mapping*, 39, 1626–1636.
- Yaesoubi, M., Miller, R. L., & Calhoun, V. D. (2017). Time-varying spectral power of resting-state fMRI networks reveal cross-frequency dependence in dynamic connectivity. *PLoS One*, 12, e0171647.
- Yang, Z., Craddock, R. C., Margulies, D. S., Yan, C. G., & Milham, M. P. (2014). Common intrinsic connectivity states among posteromedial cortex subdivisions: Insights from analysis of temporal dynamics. *NeuroImage*, 93(Pt 1), 124–137.

- Yeo, B. T., Krienen, F. M., Sepulcre, J., Sabuncu, M. R., Lashkari, D., Hollinshead, M., ... Buckner, R. L. (2011). The organization of the human cerebral cortex estimated by intrinsic functional connectivity. *Journal of Neurophysiology*, *106*, 1125–1165.
- Zeng, L. L., Wang, H., Hu, P., Yang, B., Pu, W., Shen, H., ... Hu, D. (2018). Multi-site diagnostic classification of schizophrenia using discriminant deep learning with functional connectivity MRI. *eBioMedicine*, *30*, 74–85.
- Zuo, X. N., Kelly, C., Adelstein, J. S., Klein, D. F., Castellanos, F. X., & Milham, M. P. (2010). Reliable intrinsic connectivity networks: Test-retest evaluation using ICA and dual regression approach. *NeuroImage*, *49*, 2163–2177.

SUPPORTING INFORMATION

Additional supporting information may be found online in the Supporting Information section at the end of this article.

How to cite this article: Iraj A, Deramus TP, Lewis N, et al. The spatial chronnectome reveals a dynamic interplay between functional segregation and integration. *Hum Brain Mapp.* 2019; 40:3058–3077. <https://doi.org/10.1002/hbm.24580>